Published by Institute of Physics Publishing for SISSA

Received: *June 11, 2008*
Accepted: *August 31, 2008*
Published: *September 16, 2008*

A method for the precision mass measurement of the stop quark at the International Linear Collider

Ayres Freitas,[abc] **Caroline Milstène,**[dg] **Michael Schmitt**[e] **and Andre Sopczak**[f]

[a] *University of Chicago, Chicago, IL 60637, U.S.A.*
[b] *HEP Division, Argonne National Laboratory, Argonne, IL 60439, U.S.A.*
[c] *Institut für Theoretische Physik, Universität Zürich, 8057 Zürich, Switzerland*
[d] *Fermi National Accelerator Laboratory, Batavia, IL 60510-500, U.S.A.*
[e] *Northwestern University, Evanston, IL 60208, U.S.A.*
[f] *Lancaster University, Lancaster LA1 4YB, U.K.*
[g] *Wayne State University, Detroit, MI 48202, U.S.A.*
E-mail: afreitas@physik.unizh.ch, caroline@fnal.gov, schmittm@lotus.phys.northwestern.edu, andre.sopczak@cern.ch

Abstract: Many supersymmetric models predict new particles within the reach of the next generation of colliders. For an understanding of the model structure and the mechanism(s) of symmetry breaking, it is important to know the masses of the new particles precisely. In this article the measurement of the mass of the scalar partner of the top quark (stop) at an e^+e^- collider is studied. A relatively light stop is motivated by attempts to explain electroweak baryogenesis and can play an important role in dark matter relic density. A method is presented which makes use of cross-section measurements near the pair-production threshold as well as at higher center-of-mass energies. It is shown that this method not only increases the statistical precision, but also greatly reduces the systematic uncertainties, which can be important. Numerical results are presented, based on a realistic event simulation, for two signal selection strategies: using conventional selection cuts, and using an Iterative Discriminant Analysis (IDA). Our studies indicate that a precision of $\Delta m_{\tilde{t}_1} = 0.42\,\text{GeV}$ can be achieved, representing a major improvement over previous studies. While the analysis of stops is particularly challenging due to the possibility of stop hadronization, the general procedure could be applied to the mass measurement of other particles as well. We also comment on the potential of the IDA to discover a stop quark in this scenario, and we revisit the accuracy of the theoretical predictions for the neutralino relic density.

Keywords: e+-e- Experiments.

JHEP09(2008)076

Contents

JHEP09(2008)076

1. Introduction

An experiment at the International Linear Collider (ILC) will be able to make many precise measurements from which particle properties, and ultimately, the outlines of a particle physics model may be inferred. Due to the high statistical precision expected at the ILC, the optimization of the systematic errors is of particular importance. We have studied one specific example, namely, the extraction of the mass of an hypothetical stop squark from cross-section measurements near threshold. We have devised a method which reduces most systematic uncertainties and leads to a potentially very accurate measurement of the stop squark mass. This method, however, is general and could be applied to other particles produced in an e^+e^- collider.

The method relies on the comparison of production rates at two different center-of-mass energies, and knowledge of how the cross-section varies as a function of $\sqrt{s}$ and the particle mass. In simple terms, one measures the yield at an energy close to the pair-production threshold, which will be very sensitive to the particle mass, and then at a much

higher energy, which has little sensitivity. The ratio of these two yields retains sensitivity to the mass, and at the same time is *insensitive* to many potential systematic effects.

We have chosen the case of a light scalar top squark with a mass not much higher than the mass of the lightest neutralino since production of this particle was already extensively studied in an ILC context [1, 2]. It was concluded that a conventional approach to the measurement of the stop squark mass culminated in an uncertainty of about $\Delta m_{\tilde{t}_1} = 1.2$ GeV [1, 3]. The new method substantially improves on this result, and for a similar scenario, we conclude that the uncertainty will be $\Delta m_{\tilde{t}_1} = 0.42\,\mathrm{GeV}$.

For this analysis, we have performed realistic simulations of the signal and backgrounds, and used two techniques to separate the signal from the background. The first technique is based on conventional selection cuts, while the second employs an improved Iterative Discriminant Analysis (IDA) [4]. Furthermore, the hadronization of the stop has been included and we have carefully studied the systematic uncertainties arising from this and other sources.

There are theoretical motivations for studying a light stop squark with a mass close to the neutralino mass. Specifically, we evoke a scenario within the Minimal Supersymmetric extension of the Standard Model (MSSM) which is able to explain the dark matter density of the universe as well as the baryon asymmetry through the mechanism of electroweak baryogenesis. The existence of dark matter has been firmly established by various observations, most notably by the measurements of the cosmic microwave background radiation by the Wilkinson Microwave Anisotropy Probe (WMAP) [5] and the studies conducted by the Sloan Digital Sky Survey [6]. The known properties of dark matter suggest that it consists of primordial weakly-interacting massive particles. Within the context of supersymmetry, the best candidate is the lightest neutralino, $\tilde{\chi}_1^0$, which is generically the lightest supersymmetric particle, and is stable if R-parity is conserved.

Another well-established fact which poses a great puzzle for particle physics is the apparent asymmetry between the amount of matter and anti-matter in the universe. There are several competing theoretical explanations for the origin of this baryon asymmetry. One of these relies on asymmetries generated during the electroweak phase transition. The hypothesized mechanism is not viable within the Standard Model (SM), but is possible within the context of supersymmetry. In fact, requiring that the correct baryon asymmetry is generated at the electroweak phase transition places strong constraints on the parameter space of the MSSM [7 – 10]. In particular, the lightest scalar top squark $\tilde{t}_1$ must not be heavy, satisfying the bound $m_{\tilde{t}_1} \lesssim 140\,\mathrm{GeV}$ with concomitant bounds on the mass of the Higgs boson [9, 10]. Furthermore, this particle is predominantly of the right-handed chirality state. A small mass difference between the stop and the lightest neutralino can help to bring the dark matter relic density into the proper range due to co-annihilation between the stop and the neutralino. For this mechanism to be effective, the typical mass difference is rather small, $m_{\tilde{t}_1} - m_{\tilde{\chi}_1^0} \lesssim 30$ GeV [11]. The dominant decay mode of the stop is $\tilde{t}_1 \to c\,\tilde{\chi}_1^0$, resulting in a final state with two soft charm jets and missing energy. Previous studies [1, 2] have shown that clean samples of such events can indeed be isolated at the ILC.

This paper is organized as follows. The next section explains the ratio-of-yields method

JHEP09(2008)076

in detail. Section 3 describes the tools and methods used for simulating the relevant processes and the detector, as well as two methods for selecting a clear stop signal. Section 4 is devoted to a discussion of the experimental systematics, followed by section 5 which explores theoretical uncertainties. The last section reports the results for this specific channel, and shows the implications for future calculations of dark matter relic densities based in particle physics, specifically, supersymmetry. We comment briefly on the potential of the IDA method to discover this stop quark at $\sqrt{s} = 500$ GeV. Conclusions follow.

2. Method

One way to measure the stop mass would be through kinematic distributions of its final state products. However, jet energies are difficult to measure precisely, especially when the jets are not energetic. Furthermore, the radiation of gluons and the hadronization of the stop quarks complicate the kinematics in ways that are difficult to predict and model accurately. These effects make a precise stop mass measurement from kinematic distributions rather difficult [2].

Alternatively, one can extract the stop mass and mixing angle from measurements of the cross-section. For example, it has been shown that using measurements with two different beam polarization at one center-of-mass energy, both the stop mass and mixing angle can be inferred with good accuracy [2]. For light stop quarks with masses $\mathcal{O}(100$ GeV), the typical achievable precision is $\Delta m_{\tilde{t}_1} \sim 1$ GeV. However, this technique is limited by substantial systematic uncertainties on the measurement of the total cross-section, in particular the modeling of stop hadronization and the resulting uncertainties in the selection efficiency.

We propose a new method which reduces the impact of these systematic uncertainties, and which we describe in this section in general terms. While our explication is based on the case of a light stop, the method could be applied to other particles. (See, for example, ref. [12] for a discussion of the sensitivity to unknown branching ratios.) The original presentation of this method concerned Higgs production at a future $\gamma\gamma$-collider [13].

We want to extract the mass (M_X) of a particle from measurements of its production cross sections. In order to obtain the best result, two issues must be considered:

1. optimization of the energy and luminosity for the minimum statistical error, and

2. reduction of systematic uncertainties.

The method described here seeks to address both issues in the best possible way.

The error on the extracted mass (ΔM_X) relates to the cross-section measurement error ($\Delta\sigma$) through

$$\Delta M_X = \left| \frac{d\sigma}{d\, M_X} \right|^{-1} \Delta\sigma. \tag{2.1}$$

It is important to keep in mind that the statistical component in $\Delta\sigma$ depends on σ.

For particles pair-produced mainly in the s-channel, the tree-level cross section depends on the mass through the phase space, which usually shows up as factors of the velocity of the particle: $\beta = \sqrt{1 - (M_X/E_b)^2}$ where $E_b = \sqrt{s}/2$ is the beam energy — hence, the

maximum energy the given particle can have. For the pair-production of scalar particles, $\sigma \propto \beta^3/s$, and for fermions, $\sigma \propto \beta/s$. These simple rules can be modified by radiative corrections, and by beam energy spread, but the basic picture does not change dramatically. We can use this to frame the discussion of the statistical error.

It is instructive to minimize ΔM_X as in eq. (2.1) with a simple Ansatz $\sigma = \sigma_0\beta^3/s$. We imagine that M_X is already known approximately, and we want to select the beam energy at which to run the linear collider such that ΔM_X is minimized, for a given integrated luminosity $\mathcal{L}$ and selection efficiency ϵ. One finds that $\Delta M_X = (s^2/12\sigma_0 M\beta)\Delta\sigma$. Ignoring systematic uncertainties, one might naively expect that $\Delta\sigma$ is proportional to $\sqrt{N_{\rm ev}}$, where $N_{\rm ev} = \sigma\epsilon\mathcal{L}$ is the number of selected events, which gives us $\Delta M_X \propto \sqrt{\beta}$. This surprising result indicates that zero uncertainty on the mass is obtained at the point at which the signal cross-section vanishes.

The fallacy comes in assuming that $\Delta\sigma$ is proportional to $\sqrt{N_{\rm ev}}$, which certainly does not apply as $N_{\rm ev} \to 0$, even in the absence of background. The transition from a region in which the cross-section is being measured ($\Delta\sigma \propto \sqrt{N_{\rm ev}}$) to a region in which an upper limit is being set ($N_{\rm ev} \lesssim 3$) is discussed clearly in ref. [14]. One must construct a confidence belt in the (M_X, σ) plane, for a given confidence level — 68% would be appropriate for a measurement. In the present case, this belt will depend on $\sigma(M_X)$, as well as on $\epsilon\mathcal{L}$. When the expected value for $N_{\rm ev}$ becomes too small, there is no upper bound on M_X, and eq. (2.1) clearly does not apply. In addition, an account of background estimates, of experimental uncertainties on ϵ and $\mathcal{L}$, and theoretical uncertainties on $\sigma(M_X)$ would require that one does not collect data right at threshold, but rather at a point which provides a robust signal somewhat above threshold.

Equation (2.1) still provides a useful guide in the region above threshold. We carried out a Feldman-Cousins confidence-belt construction, and obtained the statistical uncertainty ΔM_X as a function of the difference $\sqrt{s}/2 - M_X$, i.e., the energy above threshold. Figure 1 shows the result, based on the simple assumed cross-section $\sigma = \sigma_0\beta^3/s$, and approximate values for ϵ and $\mathcal{L}$ corresponding to the analysis described in section 3.2. As seen in figure 1, the uncertainty on the mass, ΔM_X, really does decrease as $\sqrt{s}/2 \to M_X$, since the sensitivity of $\sigma(M_X)$ to M_X improves more rapidly than the relative precision on the cross-section, $\Delta\sigma/\sigma$, worsens.

We turn now to a more realistic case. The theoretical cross section as a function of $\sqrt{s}$ is shown in figure 2, for two stop masses (122.5 GeV and 123.5 GeV). We include QED radiative effects, as described in section 5. Following the scenario discussed in ref. [1], we consider $M_X \approx 123$ GeV, and beam polarizations of 80% for the electron, and -60% for the positron. If we want to use a measurement of the cross section to distinguish these two masses, then clearly the threshold region is the most sensitive. This corresponds to maximizing $d\sigma/d\,M_X$, which will minimize ΔM_X according to eq. (2.1). The lower plot on the left side of figure 2 zooms in on the threshold region, to show how much the cross-section differs for two different hypothetical stop masses, and the lower plot on the right shows this difference relative to the cross-section for $m_{\tilde{t}_1} = 123$ GeV.

JHEP09(2008)076

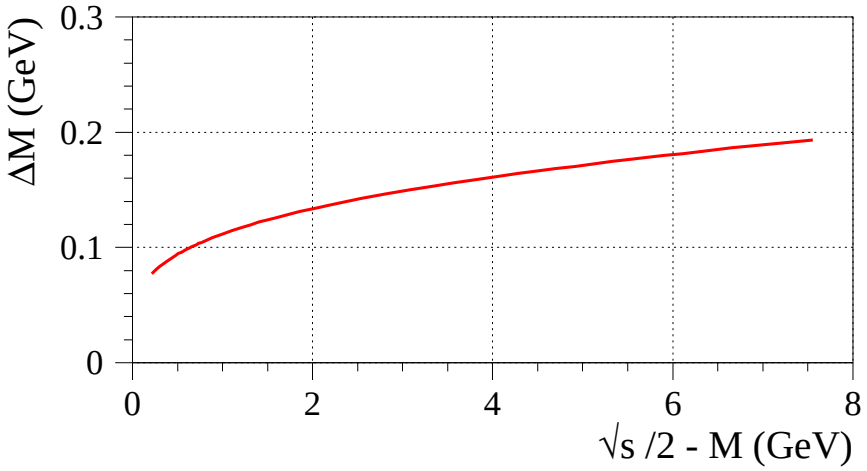

Figure 1: Statistical uncertainty on the mass, ΔM_X, as a function of the beam energy above threshold, $\sqrt{s}/2 - M_X$. This result is based on a Feldman-Cousins confidence belt construction, with a simple Ansatz for $\sigma(M_X)$ and approximate values for ϵ and $\mathcal{L}$. Backgrounds were not taken into account.

Recall the relation of the cross section to experimental quantities:

$$\sigma = \frac{N_{\rm ev} - B}{\epsilon\,\mathcal{L}} \tag{2.2}$$

where $N_{\rm ev}$ is the number of selected events, B is the estimated number of background events, ϵ is the acceptance and efficiency for the signal, and $\mathcal{L}$ is the integrated luminosity. In a real analysis, B, ϵ and $\mathcal{L}$ all carry systematic uncertainties, which must be assessed and taken into account. An 'optimal' analysis will keep these to a minimum.

Usually the most difficult component in the systematic error comes from the efficiency and acceptance. An absolute cross section requires knowledge of the absolute efficiency, which, in the case of the $\tilde{t}_1$ search described in ref. [1], involves charm-tagging as well as the hadronization and fragmentation of the $\tilde{t}_1$ and c-quark. While a large sample of $e^+e^- \to \tilde{t}_1\tilde{t}_1^*$ events will allow one to tune Monte Carlo models, and other Standard Model processes may provide large samples of c-jets for measuring efficiencies for c-tagging, it may be useful to have a method which is relatively insensitive to these sources of systematic uncertainties.

The common step toward reducing systematic uncertainties from the efficiency is to work with ratios of cross sections. This also can reduce uncertainties from the luminosity measurement, and potentially, from the background and theoretical signal cross-section as well. We propose to measure the yield of signal events close to threshold, which will be very sensitive to M_X, and compare it to the yield near the peak of the excitation curve, which will be insensitive to M_X (see figure 2). We define the observable

$$Y(M_X, \sqrt{s_{\rm th}}) \equiv \frac{N_{\rm th} - B_{\rm th}}{N_{\rm pk} - B_{\rm pk}} = \frac{\sigma_{\tilde{t}}(\sqrt{s_{\rm th}})}{\sigma_{\tilde{t}}(\sqrt{s_{\rm pk}})} \cdot \frac{\epsilon_{\rm th}}{\epsilon_{\rm pk}} \cdot \frac{\mathcal{L}_{\rm th}}{\mathcal{L}_{\rm pk}} \tag{2.3}$$

where $N_{\rm th}$ and $B_{\rm th}$ are the numbers of selected events and estimated background events for $\sqrt{s_{\rm th}}$ near threshold, and $N_{\rm pk}$, $B_{\rm pk}$ are the same quantities for $\sqrt{s_{\rm pk}}$ near the peak

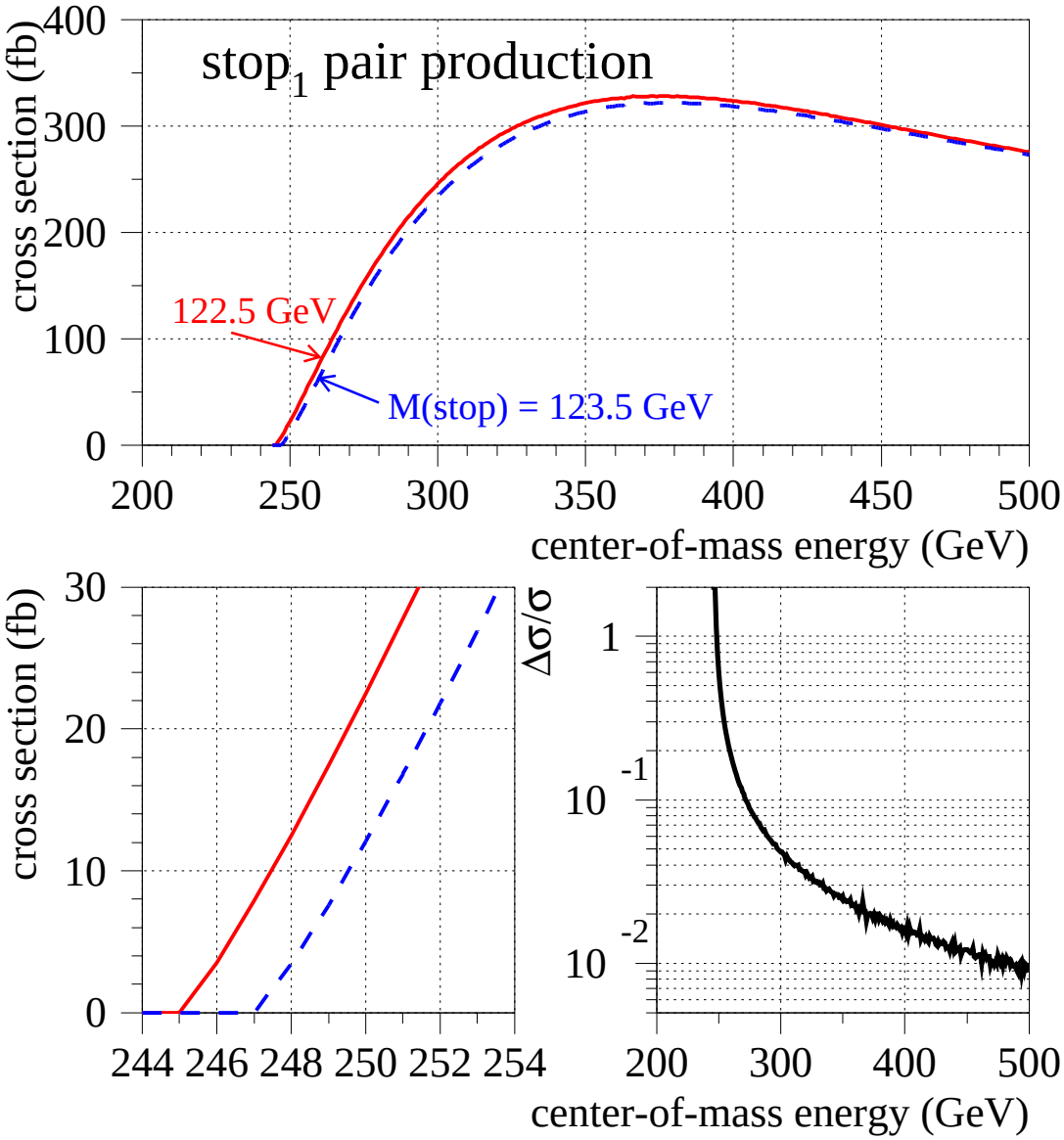

Figure 2: Cross-sections for pair production of the lightest stop squark. Top plot shows the full excitation curve as a function of $\sqrt{s}$ for two slightly different values of $m_{\tilde{t}_1}$. The lower left-hand plot shows a close-up of the threshold region. The lower right-hand plot shows the difference of the two cross-sections relative to their average value. Clearly the largest relative difference is seen very close to threshold.

of the excitation curve. Anticipating the results of later sections, we have computed the observable Y as a function of $m_{\tilde{t}_1}$, and displayed the result in figure 3.

The slope of the line in figure 3 depends on several factors, and one can attempt to optimize Y in order to obtain the best measurement of $m_{\tilde{t}_1}$. The sensitivity of Y to $m_{\tilde{t}_1}$ comes through $\sigma_{\tilde{t}}(\sqrt{s_{\rm th}})$, so $\sqrt{s_{\rm th}}$ should be close to $2m_{\tilde{t}_1}$, as discussed above. Mindful of large theoretical and growing experimental uncertainties as $\sqrt{s_{\rm th}} \to 2m_{\tilde{t}_1}$, we have selected $\sqrt{s_{\rm th}} = 260$ GeV, which is 14 GeV above the nominal threshold for a stop

JHEP09(2008)076

with $m_{\tilde{t}_1} = 123$ GeV. We find the peak cross-section occurs at $\sqrt{s_{\rm pk}} \approx 370$ GeV, but $\sqrt{s} = 500$ GeV would also serve well. Reducing the statistical uncertainty on Y to an absolute minimum would require maximizing the integrated luminosity at threshold, $\mathcal{L}_{\rm th}$, but in reality one would not run the ILC at $\sqrt{s_{\rm th}} = 260$ GeV for very long, and in practice $\mathcal{L}_{\rm th} = 50$ fb^{-1} is already adequate. We assume $\mathcal{L}_{\rm pk} = 200$ fb^{-1}.

We computed the cross sections with the program CALVIN [15], which includes next-to-leading (NLO) order supersymmetric QCD corrections, and which was modified for this work to include resummed Coulomb corrections near threshold (see section 5). For two common choices of beam polarization, the cross-sections are

$$\begin{aligned} P(e^-) = -80\%/P(e^+) = +60\%: &\quad \sigma(\sqrt{s_{\rm th}}) = 17.4 \text{ fb} \quad \sigma(\sqrt{s_{\rm pk}}) = 72 \text{ fb}, \\ P(e^-) = +80\%/P(e^+) = -60\%: &\quad \sigma(\sqrt{s_{\rm th}}) = 77 \text{ fb} \quad\;\; \sigma(\sqrt{s_{\rm pk}}) = 276 \text{ fb}, \end{aligned} \tag{2.4}$$

where $P < 0$ stands for left-handed polarization and $P > 0$ for right-handed polarization. We choose the second set of polarization values since it leads to a much better signal-to-background ratio.

For the computation of the observable Y depicted in figure 3, we employed the results of the "cut-based" analysis described in section 3.2. The efficiencies at threshold and peak are $\epsilon_{\rm th} = 0.34$ and $\epsilon_{\rm pk} = 0.21$ (see table 3), and the total background cross-sections are 2.5 fb and 10.3 fb (see table 4), respectively. The strong variation of Y with $m_{\tilde{t}_1}$ in figure 3 indicates that a precise measurement of Y will lead to a precise value for $m_{\tilde{t}_1}$. The shaded horizontal band corresponds to a 3% uncertainty on Y, resulting in $\Delta m_{\tilde{t}_1} = 0.2$ GeV, which would be far better than the result reported in ref. [1].

We consider now the impact of systematic uncertainties on the observable Y, and eq. (2.3) provides our starting point. For the event selection criteria described in sections 3.2 and 3.3, the signal is much bigger than the background, so the main experimental uncertainties will come from ϵ. The values for ϵ at threshold and on the peak come from Monte Carlo simulations of the signal process. Systematic errors arise when these simulations do not match reality perfectly. For example, the calibration of the calorimeter energy measurement for real data may be slightly different than is simulated, in which case the efficiency for a cut on the total visible energy $E_{\rm vis}$ as estimated from the simulation will be slightly incorrect. One can express the impact of this error on the efficiency as $\epsilon^{\rm true} = \epsilon^{\rm est}(1+\delta)$, so that δ is the *relative* shift in the efficiency. Then the impact on the observable Y is simply

$$Y^{\rm true} = Y^{\rm est}\left(\frac{1+\delta_{\rm th}}{1+\delta_{\rm pk}}\right) \qquad \frac{Y^{\rm true} - Y^{\rm est}}{Y^{\rm true}} \approx \delta_{\rm pk} - \delta_{\rm th}.$$

Thus, if the systematic uncertainties $\delta_{\rm pk}$ and $\delta_{\rm th}$ are correlated, and if they have the same relative impact on $\epsilon_{\rm pk}$ and $\epsilon_{\rm th}$, the net effect on Y will be zero, and there will be no error on $m_{\tilde{t}_1}$. For some systematic effects, the errors will be correlated, but of a different magnitude at the two energies, so that the cancellation $|\delta_{\rm pk} - \delta_{\rm th}|$ will not be complete. For other systematic effects, the errors will be uncorrelated, in which case there is no cancellation. Clearly the analysis should be designed in such a way as to take advantage of this cancellation. In practice, this means that the cuts should have a similar impact on the

JHEP09(2008)076

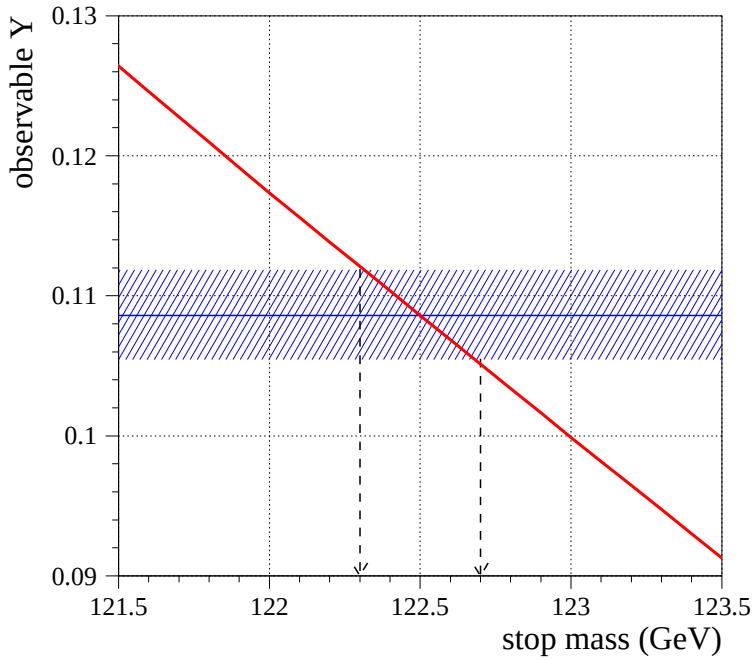

Figure 3: Variation of observable Y with $m_{\tilde{t}_1}$, shown by the solid red line. The horizontal line gives the expected value of Y when $m_{\tilde{t}_1} = 122.5$ GeV, and the shaded band shows a variation of Y by 3%. The vertical arrows indicate the corresponding uncertainty on $m_{\tilde{t}_1}$.

signal at both energies. For the present application, there is a large degree of cancellation, leading to a greatly reduced systematic uncertainty on the observable Y, and hence on $m_{\tilde{t}_1}$. The details are given in section 4.

We proceed now to a detailed and realistic simulation, and the description of two fully-developed event selection methods.

3. Event selection and analysis

At an e^+e^- collider, scalar top quarks would be produced in pairs, and decay to a c-quark and the lightest neutralino:

$$e^+e^- \to \tilde{t}_1\,\tilde{t}_1^* \to c\tilde{\chi}_1^0\,\bar{c}\tilde{\chi}_1^0. \tag{3.1}$$

The stop quarks live long enough to hadronize before decaying, so the final state signature consists of two charm quark jets, missing energy and possibly additional jets due to the hadronization process and gluon radiation.

In the following sections, the method described in section 2 will be applied to the theoretical parameter point of ref. [3] which has the same stop and neutralino masses and mixings as the study of ref. [1]. The weak-scale MSSM parameters are

$$\begin{aligned} m^2_{\tilde{\mathrm{U}}_3} &= -99^2 \text{ GeV}, & m_{\tilde{\mathrm{Q}}_3} &= 4330 \text{ GeV}, & m_{\tilde{\mathrm{Q}},\tilde{\mathrm{U}},\tilde{\mathrm{D}},\tilde{\mathrm{L}},\tilde{\mathrm{R}}_{1,2}} &= 10 \text{ TeV}, \\ M_1 &= 118.8 \text{ GeV}, & M_2 &= 225 \text{ GeV}, & |\mu| &= 225 \text{ GeV}, \\ A_t &= -1100 \text{ GeV}, & m_{\mathrm{A}^0} &= 800 \text{ GeV}, & \phi_\mu &= 0.2, \qquad \tan\beta = 5. \end{aligned} \tag{3.2}$$

The corresponding tree-level masses are:

$$\begin{aligned} & & m_{\tilde{t}_1} = 122.5 \text{ GeV}, & & m_{\tilde{t}_2} = 4333 \text{ GeV}, & \\ m_{\tilde{\chi}^0_1} = 107.2 \text{ GeV}, & & m_{\tilde{\chi}^0_2} = 170.8 \text{ GeV}, & & m_{\tilde{\chi}^0_3} = 231.2 \text{ GeV}, & m_{\tilde{\chi}^0_4} = 297.7 \text{ GeV}, \\ & & m_{\tilde{\chi}^\pm_1} = 162.7 \text{ GeV}, & & m_{\tilde{\chi}^\pm_2} = 296.2 \text{ GeV}, & \end{aligned} \tag{3.3}$$

and the light stop state is almost completely right-chiral, $\cos\theta_{\tilde{t}} = 0.010$. As a result of the small stop-neutralino mass difference, the stop almost completely decays through the loop-induced process into a charm and neutralino, $\tilde{t} \to c\,\tilde{\chi}^0_1$. Due to the loop suppression of the decay, the stop is expected to hadronize before decaying. We have carried out realistic experimental simulations, and will present the analysis of relevant systematic effects.

3.1 Simulation

Both the signal and background events are generated with Pythia 6.129 [16]. The cross-sections for the signal process were computed with Calvin [15] with some improvements as in ref. [17]. The relevant background processes have been computed by adapting the Monte Carlo code used in ref. [17] and by Grace 2.0 [18], with cross-checks with CompHep 4.4 [19]. The simulation and cross-section calculations incorporated beamstrahlung for cold ILC technology as parameterized in the program Circe 1.0 [20]. Table 1 summarizes the predicted signal and background cross-sections. To avoid the infrared divergence of the two-photon background process, a cut on the minimal transverse momentum is applied, $p_T > 5\,\text{GeV}$. Backgrounds from supersymmetric processes will be discussed below. Table 2 lists the numbers of events generated and equivalent luminosity based on the cross-sections in table 1.

Hadronization of the final state charm quark and the intermediate stop quark are a key issue in this study. The Lund string fragmentation model was used together with the Peterson fragmentation function [21]. The stop fragmentation is simulated [22] by labeling the stop quark as a stable particle in an intermediate step, and switching on the stop decay again after stop fragmentation. The modeling of the hadronization spectrum of the stop is described in ref. [23]. The dominant lightest stop hadron states are mesons composed of a stop and an up or down quark.

The Simdet detector simulation [24] was used, describing a typical ILC detector. The analysis used the N-Tuple tool [25], which incorporates jet-finding algorithms. In order to reduce the size of the ntuples, several pre-selection cuts were applied, as was done for the previous analysis [1]:

$$\begin{aligned} 4 < N_{\text{tracks}} < 50, & \qquad p_T > 5 \text{ GeV}, \\ |\cos\theta_{\text{thrust}}| < 0.8, & \qquad |p_L/p_{\text{tot}}| < 0.9, \\ E_{\text{vis}} < 0.75\sqrt{s}, & \qquad m_{\text{inv}} < 200 \text{ GeV}. \end{aligned} \tag{3.4}$$

These quantities are all global event quantities computed from the energy flow algorithm. p_T, p_L and p_{tot} are computed from all energy flow objects, as are E_{vis} and m_{vis}. N_{tracks} is the number of reconstructed charged tracks, and the thrust axis is found from all energy flow objects. Most of these cuts have very little impact on the signal efficiency.

JHEP09(2008)076

Process	Cross-section [pb] at $\sqrt{s_{\rm th}}$=260 GeV			Cross-section [pb] at $\sqrt{s_{\rm pk}}$=500 GeV		
$P(e^-)/P(e^+)$	0/0	−80%/+60%	+80%/−60%	0/0	−80%/+60%	+80%/−60%
$\tilde{t}_1\tilde{t}_1^*$	0.032	0.017	0.077	0.118	0.072	0.276
W^+W^-	16.9	48.6	1.77	8.6	24.5	0.77
ZZ	1.12	2.28	0.99	0.49	1.02	0.44
$We\nu$	1.73	3.04	0.50	6.14	10.6	1.82
eeZ	5.1	6.0	4.3	7.5	8.5	6.2
$q\bar{q}$, $q \neq t$	49.5	92.7	53.1	13.1	25.4	14.9
$t\bar{t}$	0.0	0.0	0.0	0.55	1.13	0.50
2-photon $p_T > 5\,\text{GeV}$	786			936		

Table 1: Total cross sections for the stop signal and Standard Model background processes for $\sqrt{s_{\rm th}} = 260$ GeV and $\sqrt{s_{\rm pk}} = 500$ GeV and different combinations of beam polarization. The signal is given for a right-chiral stop of $m_{\tilde{t}_1} = 122.5$ GeV. Negative polarization values refer to left-handed polarization and positive values to right-handed polarization. No branching ratios for W and Z bosons are imposed.

	$\sqrt{s_{\rm th}} = 260$ GeV			$\sqrt{s_{\rm pk}} = 500$ GeV		
	generated	luminosity (fb^{-1})		generated	luminosity (fb^{-1})	
$P(e^-)/P(e^+)$		0/0	+80%/−60%		0/0	+80%/−60%
$\tilde{t}_1\tilde{t}_1^*$	50,000	1562	649	50,000	423	181
W^+W^-	180,000	11	102	210,000	24	273
ZZ	30,000	27	30	30,000	61	68
$We\nu$	210,000	121	420	210,000	34	115
eeZ	210,000	41	49	210,000	28	34
$q\bar{q}$, $q \neq t$	350,000	7	6	350,000	27	23
$t\bar{t}$	—	—	—	180,000	327	360
2-photon	1.6×10^6	2	2	8.5×10^6	9	9

Table 2: Numbers of generated events at $\sqrt{s_{\rm th}} = 260$ GeV and $\sqrt{s_{\rm pk}} = 500$ GeV, and the equivalent luminosities in fb^{-1}.

3.2 Sequential-cut analysis

Although Standard Model background processes are several orders of magnitude larger than the stop signal process, the background contributions can be reduced to an acceptable level by suitable selection cuts. This work follows the analysis of ref. [1], but makes some adjustments to accommodate the stop fragmentation effects, and to take advantage of the cancellation of systematic uncertainties as discussed in section 2.

JHEP09(2008)076

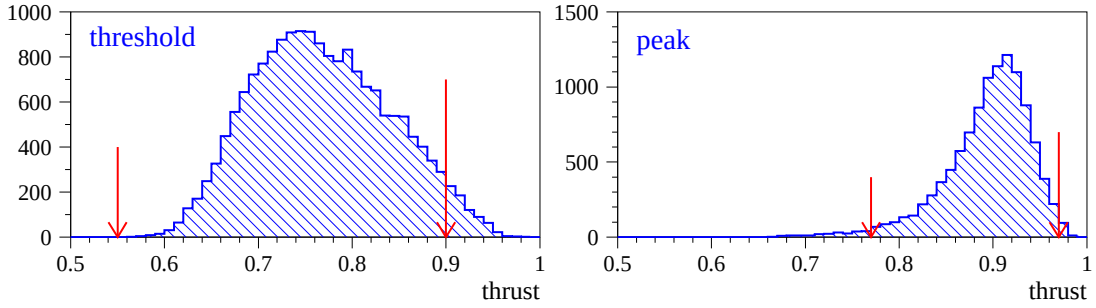

Figure 4: Signal marginal distributions for the thrust, at $\sqrt{s_{\rm th}}$ (left) and at $\sqrt{s_{\rm pk}}$ (right). The arrows indicate the cuts chosen to minimize the systematic uncertainties as well as the statistical uncertainty.

The event selection begins with some basic and common kinematic cuts based on global event quantities. The visible energy, $E_{\rm vis}$, must be less than $0.3\sqrt{s}$ to ensure a large missing-energy signature. It must be greater than $0.1\sqrt{s}$ to suppress the bulk of the two-photon events. Similarly, the number of reconstructed charged tracks should indicate real hadronic jets, so we require $N_{\rm tracks} \geq 5$. In order to suppress $We\nu$ and $q\bar{q}$ signals, we place an upper bound $N_{\rm tracks} \leq 25$ at threshold and $N_{\rm tracks} \leq 20$ at peak. These cuts on $N_{\rm tracks}$ remove only a couple of percent of the signal.

We place one more kinematic and one topological cut to further reduce the backgrounds. The cuts values are carefully tuned to achieve a low systematic uncertainty for the observable Y, as well as a good background rejection. In practice, this means aiming to remove approximately the same amount of signal at the two center-of-mass energies, rather than achieving the highest signal efficiencies. In particular, the efficiency at $\sqrt{s_{\rm pk}}$ is relatively unimportant since we anticipate a large luminosity and a large signal cross-section there. The thrust value, computed from all energy-flow objects, is useful for eliminating $q\bar{q}$ and two-photon events. As shown in figure 4, the thrust distribution for the signal is rather different at the two center-of-mass energies, so we require $0.77 \leq T \leq 0.97$ at $\sqrt{s_{\rm th}}$ and $0.55 \leq T \leq 0.90$ at $\sqrt{s_{\rm pk}}$. Similarly, the event p_T, calculated from all energy flow objects in the event, is crucial for eliminating the two-photon background. Our study indicates that a minimum cut $p_T > 15$ GeV is needed. We tighten this cut to $p_T > 22$ GeV at $\sqrt{s_{\rm pk}}$ in order to eliminate the same amount of signal events as are eliminated at $\sqrt{s_{\rm th}}$. Figure 5 shows that cutting at $p_T = 22$ GeV at $\sqrt{s_{\rm pk}}$ places the cut at almost the same point in the p_T distribution for both center-of-mass energies. An upper cut on p_T helps reduce the $We\nu$ background, so we require $p_T < 45$ GeV at $\sqrt{s_{\rm th}}$ and $p_T < 50$ GeV at $\sqrt{s_{\rm pk}}$, which again reflects our effort to minimize the systematic uncertainty.

One might expect that the signal process (3.1) produces only two jets. However, additional soft jets can emerge from the stop hadronization process and also from the decay of the stop hadron. In order to maintain a high efficiency, and to avoid large systematic uncertainties from the modeling of the rate and characteristics of these extra jets, events with more than two jets should not be rejected. However, to suppress the background processes effectively, extra jets are allowed only when their energy falls below a certain

JHEP09(2008)076

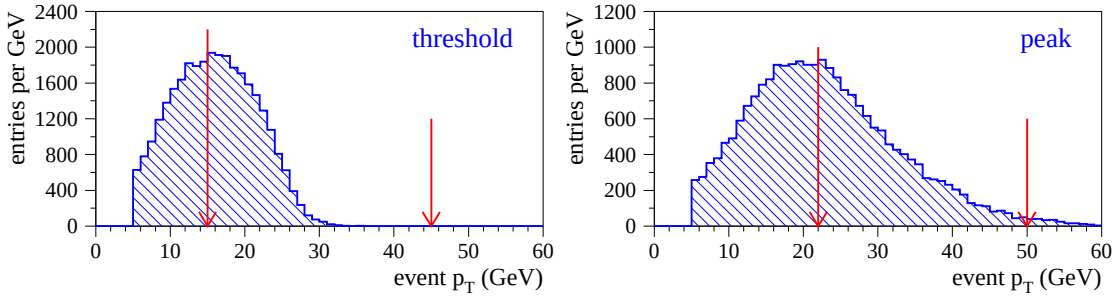

Figure 5: Signal marginal distributions for p_T, at $\sqrt{s_{\rm th}}$ (left) and at $\sqrt{s_{\rm pk}}$ (right). The arrows indicate the cuts chosen to minimize the systematic uncertainties as well as the statistical uncertainty.

cut-off value. To be specific, if there are more than two jets in an event, only two of the jets are allowed to have energies above 25 GeV. In this paper, we refer to this requirement as the "extra-jet veto." Furthermore, if there are more than three jets, the most energetic jet cannot be too energetic — its energy must be less than 35 GeV. These cuts are useful against the troublesome $We\nu$ backgrounds, especially at $\sqrt{s_{\rm pk}}$.

Further substantial improvements of the signal-to-background ratio can be achieved by exploiting kinematic and topological correlations between the two c-quark jets. Therefore it is necessary to identify them from the plurality of jets, and for this we use charm tagging as realized using a neural network [26]. The neural network uses information about the vertex position of a jet based on a topological vertex finder, the impact parameter probability, the momenta of the associated tracks and the reconstructed mass. It has been optimized to single out charm jets with an energy that is typical for light stops, while rejecting light quark jets coming from $We\nu$ background. Each jet in an event is tested with the charm tagger, and a charm flag $F_i^{(c)}$ is set (ideally, $F_i^{(c)} = 1$ indicates a charm jet). First, if a displaced vertex is reconstructed, the jet is tagged positively with $F_i^{(c)} = 1$. A displaced vertex is found roughly 50% of the time for a charm jet, and less than 20% of the time for a light quark jet. If no such vertex is reconstructed, then the neural network is employed, which produces a charm flag value between zero and one, $0 \leq F_i^{(c)} \leq 1$. The output of the neutral network is shown in figure 6, for the second of the two charm-tagged jets.

We consider the two jets in the event with the highest values of $F_i^{(c)}$, and require $P_{\rm c} \equiv F_1^{(c)} \times F_2^{(c)} > 0.6$, which is very effective at eliminating events with no charm-quark jets while retaining a high efficiency for signal events. In particular, the $We\nu$ background is reduced by more than half. Figure 7 compares the quantity $P_{\rm c}$ for signal events and $We\nu$ background which have passed the kinematic event selection cuts. Since half of the $We\nu$ events have a genuine charm jet, it is the value of $F_i^{(c)}$ for the second jet which best distinguishes signal and background.

A further substantial reduction can be obtained from cuts on the invariant mass of the two best charm-tagged jets — we veto events in which that mass is consistent with the W-boson mass.

JHEP09(2008)076

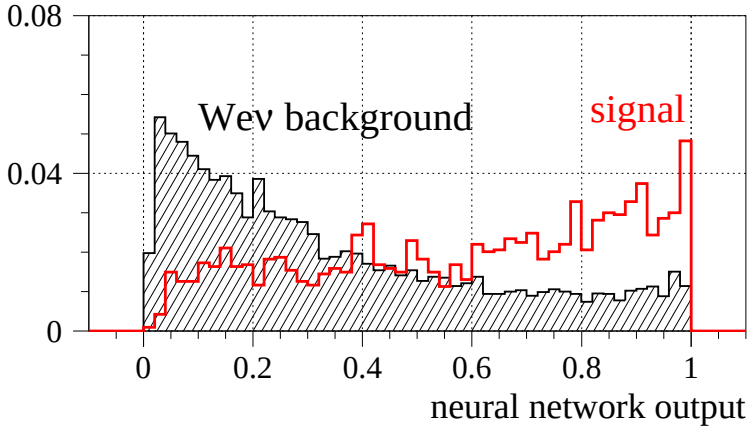

Figure 6: Illustration of the ability of the neural network to discriminate signal and the main background coming from $We\nu$ production, for the second of two charm-tagged jets. Both distributions are normalized to unit area.

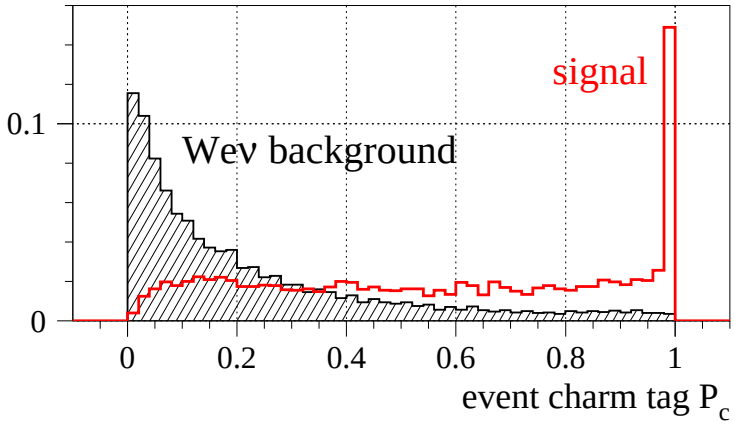

Figure 7: Event charm probability, $P_c = F_1^{(c)} \times F_2^{(c)}$, comparing signal and the $We\nu$ background. Our requirement is $P_c > 0.6$. These distributions are normalized to unit area.

The event selection cuts are summarized in table 3, for the two center-of-mass energies, $\sqrt{s_{\rm th}} = 260$ GeV and $\sqrt{s_{\rm pk}} = 500$ GeV. These follow the pre-selection cuts listed in eq. (3.4).

Our estimates of the numbers of signal and background events surviving the cuts listed in table 3 are summarized in table 4. If, in a given channel, no simulated events remain after applying our cuts, we list an upper limit corresponding to one simulated event, and we count this amount in the total background estimate. As evident from the table, the background can be greatly reduced for $\sqrt{s_{\rm th}}$, resulting in a very good signal-to-background ratio. At $\sqrt{s_{\rm pk}}$, on the other hand, a large background from single-W boson production is left. For unpolarized beams, the resulting signal-to-background ratio is 0.7. While this would allow an unambiguous discovery of stop quarks (see section 6.4), it is not a very good basis for precision measurements of the stop mass. Fortunately, the signal-to-background ratio can be greatly improved by using polarized beams. With an essentially right-handed electron

JHEP09(2008)076

Variable	$\sqrt{s_{\rm th}} = 260$ GeV	$\sqrt{s_{\rm pk}} = 500$ GeV
number of charged tracks	$5 \le N_{\rm tracks} \le 25$	$5 \le N_{\rm tracks} \le 20$
visible energy $E_{\rm vis}$	$0.1 < E_{\rm vis}/\sqrt{s} < 0.3$	$0.1 < E_{\rm vis}/\sqrt{s} < 0.3$
event longitudinal momentum	$\lvert p_L/p_{\rm tot}\rvert < 0.85$	$\lvert p_L/p_{\rm tot}\rvert < 0.85$
event transverse momentum p_T	$15 < p_T < 45\,\text{GeV}$	$22 < p_T < 50\,\text{GeV}$
thrust T	$0.77 < T < 0.97$	$0.55 < T < 0.90$
number of jets $N_{\rm jets}$	$N_{\rm jets} \ge 2$	$N_{\rm jets} \ge 2$
extra-jet veto	$E_{\rm jet} < 25\,\text{GeV}$	$E_{\rm jet} < 25\,\text{GeV}$
charm tagging likelihood $P_{\rm c}$	$P_{\rm c} > 0.6$	$P_{\rm c} > 0.6$
di-jet invariant mass $m_{\rm jj}$	$m^2_{\rm jj} < 5500\ \text{GeV}^2$ or $m^2_{\rm jj} > 8000\ \text{GeV}^2$	$m^2_{\rm jj} < 5500\ \text{GeV}^2$ or $m^2_{\rm jj} > 10000\ \text{GeV}^2$
signal efficiency	0.340	0.212

Table 3: Selection cuts for $\sqrt{s_{\rm th}} = 260$ GeV and $\sqrt{s_{\rm pk}} = 500$ GeV. Also listed are the selection efficiencies for right-chiral stop squarks and neutralinos with masses given in eq. (3.3). See the text for explanations of the extra-jet veto, charm tagging, and the $m^2_{\rm jj}$ cut.

	$\sqrt{s_{\rm th}} = 260$ GeV		$\sqrt{s_{\rm pk}} = 500$ GeV	
	$\mathcal{L} = 50\ \text{fb}^{-1}$		$\mathcal{L} = 200\ \text{fb}^{-1}$	
$P(e^-)/P(e^+)$	0/0	+80%/−60%	0/0	+80%/−60%
$\tilde{t}_1\tilde{t}_1^*$	544	1309	5170	12093
W^+W^-	38	4	16	2
ZZ	8	7	36	32
$We\nu$	208	60	7416	2198
eeZ	2	2	< 7	< 6
$q\bar{q}$, $q \neq t$	42	45	15	17
$t\bar{t}$	0	0	7	7
2-photon	53	53	12	12
total background	351	171	7509	2274
S/B	1.5	7.6	0.7	5.3

Table 4: Expected numbers of events remaining at $\sqrt{s_{\rm th}} = 260$ GeV and $\sqrt{s_{\rm pk}} = 500$ GeV, with unpolarized and with polarized beams, after sequential selection cuts have been applied. The entries in the form $< N$ show the number of events corresponding to a single selected simulated event.

beam and left-handed positron beam, the signal is enhanced, while most backgrounds are substantially suppressed. As a result, the signal-to-background ratio at $\sqrt{s_{\rm pk}} = 500$ GeV is improved from 0.7 to 5.3. Our studies are based on these assumed beam polarizations, giving us total background cross sections of 2.5 fb and 10.3 fb at the two energies.

JHEP09(2008)076

We checked for possible supersymmetric backgrounds. The main concern is chargino pair production with the decay channel $\tilde{\chi}_1^+ \to \tilde{t}_1 b$. We simulated a sample of these decays, consistent with our benchmark scenario, and found that the cuts listed in table 3 completely eliminate this background source.

With the results listed in table 4 for polarized beams, we can compute the observable Y and its statistical error, obtaining $Y = 0.1082 \pm 0.0034$ with a relative error of 3.1%. The corresponding stop quark mass would be

$$m_{\tilde{t}_1} = (122.5 \pm 0.19)\ \text{GeV} \tag{3.5}$$

where the uncertainty depends on the slope, $dY/dM = -0.01755$, at $Y = 0.1082$. Without positron polarization, $P(e^+) = 0$, the precision of the measurement is reduced by roughly 20%, resulting in $\Delta Y/Y = 3.7\%$ and $\Delta m_{\tilde{t}_1} = 0.23$ GeV. Even in this case the statistical error is rather small.

It should be recalled that the production cross-section is a strong function of the mixing angle, so the statistical error $\Delta m_{\tilde{t}_1}$ will also depend on it. In our reference scenario, the light stop eigenstate is almost completely composed of the partner of the right-handed top quark, $\tilde{t}_1 \approx \tilde{t}_\mathrm{R}$, with the mixing angle $\cos\theta_{\tilde{t}} = 0.01$. While this scenario is preferred by electroweak precision data and the explanation of baryogenesis, an experimental analysis should consider all possible values for the stop mixing angle. For other values of $\cos\theta_{\tilde{t}}$, the production cross-section can change drastically, depending on the beam polarization. As a concrete example, we consider two larger values of $\cos\theta_{\tilde{t}}$:

$$\begin{aligned} \cos\theta_{\tilde{t}} = 0.6: \quad & \sigma_{\mathrm{L},260} = 52\,\mathrm{fb}, & \sigma_{\mathrm{L},500} = 194\,\mathrm{fb}, \\ & \sigma_{\mathrm{R},260} = 39\,\mathrm{fb}, & \sigma_{\mathrm{R},500} = 148\,\mathrm{fb}, \end{aligned} \tag{3.6}$$

$$\begin{aligned} \cos\theta_{\tilde{t}} = 1.0: \quad & \sigma_{\mathrm{L},260} = 169\,\mathrm{fb}, & \sigma_{\mathrm{L},500} = 577\,\mathrm{fb}, \\ & \sigma_{\mathrm{R},260} = 6.9\,\mathrm{fb}, & \sigma_{\mathrm{R},500} = 30\,\mathrm{fb}. \end{aligned} \tag{3.7}$$

Here $\sigma_{\mathrm{L/R},E}$ stands for the stop production cross-section at center-of-mass energy E GeV, and with beam polarization combinations $P(e^-) = -80\%/P(e^+) = +60\%$ and $P(e^-) = +80\%/P(e^+) = -60\%$, respectively. If the stop is dominantly left-chiral, with $|\cos\theta_{\tilde{t}}| > 0.5$, the production cross-section is substantially larger for left-handed electron and right-handed positron polarization, opposite to the situation for a right-chiral stop. Therefore, for large values of $|\cos\theta_{\tilde{t}}|$, it is better to use the beam polarizations $P(e^-) = -80\%/P(e^+) = +60\%$, even though one has to deal with much larger Standard Model background. The largest background, $e^+e^- \to We\nu$, amounts to about 12800 events at $\sqrt{s} = 500$ GeV and $\mathcal{L} = 200$ fb^{-1} for this polarization. Nevertheless, due to large signal cross-sections, the resulting statistical error is still small, as summarized in table 5, which demonstrates that, for all values of the stop mixing angle, one can measure the stop mass with a statistical error better than 0.3 GeV using our method and an appropriate choice of beam polarization.

3.3 Iterative discriminant analysis

A traditional, sequential-cut analysis was presented in the previous section. Often, more advanced multi-variate techniques can boost the sensitivity of a search. We investigated

$\cos\theta_{\tilde{t}}$	$P(e^-) = -80\%/P(e^+) = +60\%$	$P(e^-) = +80\%/P(e^+) = -60\%$
0.0	0.69	**0.19**
0.6	0.29	**0.28**
1.0	**0.14**	0.94

Table 5: Statistical uncertainties $\Delta m_{\tilde{t}_1}$ in GeV, for selected values of $\cos\theta_{\tilde{t}}$ and two opposite sets of beam polarization. The bold numbers indicate the best choice of beam polarization for the given value of the stop mixing angle.

the efficacy of an Iterative Discriminant Analysis (IDA) for the purposes of measuring the stop quark mass based on the observable Y.

The IDA method [4] is a modified Fisher Discriminant Analysis, the two main differences are the introduction of a non-linear discriminant function and iterations in order to enhance the separation of signal and background. Two IDA steps have been performed. In order to have two independent samples for the derivation of the IDA function and for the expected performance, the signal and background samples were divided into two equally-sized samples. For this analysis, the same kinematic variables and simulated event samples as in the cut-based analysis are used, including the charm tagging flags $F_i^{(c)}$. Before the multi-variable analysis is performed, cuts on the input variables reduce the number of events presented to the IDA. This reduces the computational time needed for optimization, and leads to an improved performance by removing events that are not at all signal-like. From the distributions of the input variables for the signal and background events, the IDA method calculates a separating surface in the multi-dimensional parameter space between signal and background events. The IDA output variable has a different shape for signal and background events, and therefore a cut on this variables is used to separate signal and background. In the first IDA step a cut is placed on this IDA output variable such that 99.5% of the signal efficiency are kept. The number of background events is largely reduced. From the smaller background sample and the 99.5% remaining signal events again a new IDA output variable is constructed. The cut on the IDA output variable in this second IDA step defines the signal efficiency and the corresponding number of background events. Different working points are possible: they are defined by choosing a certain signal efficiency and obtaining the corresponding number of background events. The working point was determined by the expected error on $m_{\tilde{t}_1}$. The results of the IDA method with stop fragmentation are shown in figure 8 and table 6 expressed as number of expected background events for each contributing background process.

As before, in the channels where no event is left after the signal selection, an upper limit corresponding to one simulated event is given in the table.

The IDA method achieves a significantly more powerful discrimination between signal and background than the analysis with conventional cuts. When allowing similar background levels as for the cut-based analysis in table 4, signal efficiencies of $\epsilon_{\rm th} = 0.387$ for $\sqrt{s_{\rm th}} = 260$ GeV and $\epsilon_{\rm pk} = 0.416$ for $\sqrt{s_{\rm pk}} = 500$ GeV are obtained.

With the resulting event numbers given in table 6 for $P(e^-)/P(e^+) = +80\%/-60\%$,

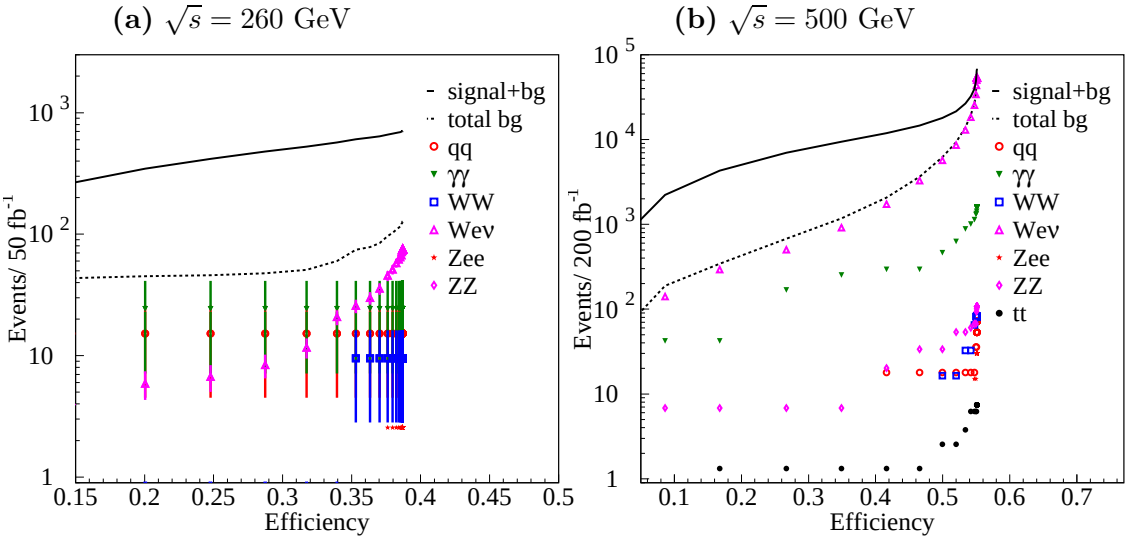

Figure 8: Performance of the Iterative Discriminant Analysis (IDA) for $\sqrt{s} = 260$ GeV and $\sqrt{s} = 500$ GeV. The plots show the remaining background event numbers for unpolarized beams as a function of the signal efficiency.

	$\sqrt{s_{\rm th}} = 260$ GeV		$\sqrt{s_{\rm pk}} = 500$ GeV	
	$\mathcal{L} = 50$ fb^{-1}		$\mathcal{L} = 200$ fb^{-1}	
$P(e^-)/P(e^+)$	0/0	+80%/−60%	0/0	+80%/−60%
$\tilde{t}_1\tilde{t}_1^*$	619	1489	9815	22958
W^+W^-	11	1	< 8	< 1
ZZ	< 2	< 2	20	18
$We\nu$	68	20	1719	510
eeZ	3	2	< 7	< 6
$q\bar{q}$, $q \neq t$	16	17	18	21
$t\bar{t}$	0	0	1	1
2-photon	27	27	294	294
total background	127	69	2067	851
S/B	4.9	22	4.7	27

Table 6: As in table 4, expected numbers of events remaining at $\sqrt{s_{\rm th}} = 260$ GeV and $\sqrt{s_{\rm pk}} = 500$ GeV, with unpolarized and with polarized beams, after the IDA has been applied.

the ratio quantity in eq. (2.3) amounts to $Y = 0.0648 \pm 0.0018$ with a relative statistical error of 2.7%, translating into

$$m_{\tilde{t}_1} = (122.5 \pm 0.17)\ \text{GeV} \tag{3.8}$$

where the uncertainty on the mass depends on the slope $dY/dM = -0.01052$. The higher

JHEP09(2008)076

signal efficiency and lower background achieved by the two-step IDA results in a slightly smaller statistical uncertainty (*cf.* eq. (3.5)).

4. Experimental systematics

The high signal efficiency and low backgrounds achieved in both the cut-based analysis (section 3.2) and the IDA (section 3.3) deliver an excellent statistical precision — $\Delta m_{\tilde{t}_1} < 0.2$ GeV. It remains to investigate systematic uncertainties, which were the dominant contribution in the previous analysis of ref. [1]. We considered the following important sources of systematic errors:

- detector calibration (energy scale)
- charm tagging
- hadronization / fragmentation
- neutralino mass
- luminosity measurement
- beam energy spectrum
- background estimate

The first four sources pertain to the signal efficiency. We discuss these sources in detail in the context of the sequential-cut analysis detailed in section 3.2 first, and then briefly report the results obtained from the IDA method described in section 3.3.

4.1 Systematics for the sequential-cut analysis

Many of the kinematic quantities used in these selections depend on a correct calibration of the calorimetry. Based on experience from LEP [27], we assume an uncertainty of 1% on the overall energy scale, which is rather pessimistic for a future ILC detector. We scaled simultaneously all kinematic quantities through a range of ±6% and observed correlated shifts in the overall selection efficiency at the two center-of-mass energies. In particular, the p_T cut is sensitive to this kind of scale error, prompting us to tune the cut at $\sqrt{s_{\rm pk}}$ to achieve a minimal residual uncertainty for the *ratio* of efficiencies, as discussed in section 3.2.

Figure 9 shows how the selection efficiencies change as a function of the scale factor. Using our optimized p_T cut shown in figure 5, one sees a parallel behavior at threshold (upper solid line) and at peak (lower solid line). This leads to a very good cancellation for the ratio of efficiencies, as shown by the solid line in figure 10. If we had optimized for efficiency only, then we would have used nearly the same p_T cuts at the peak as we use at threshold. However, this would have given a rather different dependence on the scale, as indicated by the dashed line in figure 9, and therefore a much stronger dependence of the ratio of efficiencies on the scale, as shown by the dashed line in figure 10. With our best cuts, an uncertainty of ±1% on the calorimeter energy scale translates into an uncertainty of less than 0.6% on the ratio of efficiencies.

JHEP09(2008)076

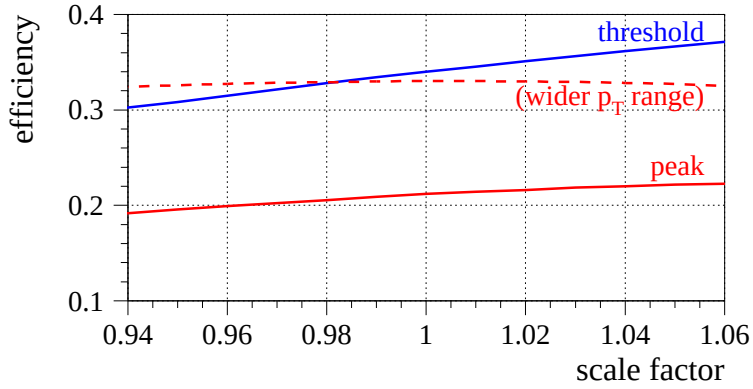

Figure 9: Variation of the selection efficiencies ($\epsilon_{\rm th}$ and $\epsilon_{\rm pk}$) with an overall energy scale factor. The two solid lines show the variation obtained with our nominal cuts, at $\sqrt{s_{\rm th}}$ and $\sqrt{s_{\rm pk}}$. The dashed line shows what we would obtain if we applied a looser p_T cut at $\sqrt{s_{\rm pk}}$.

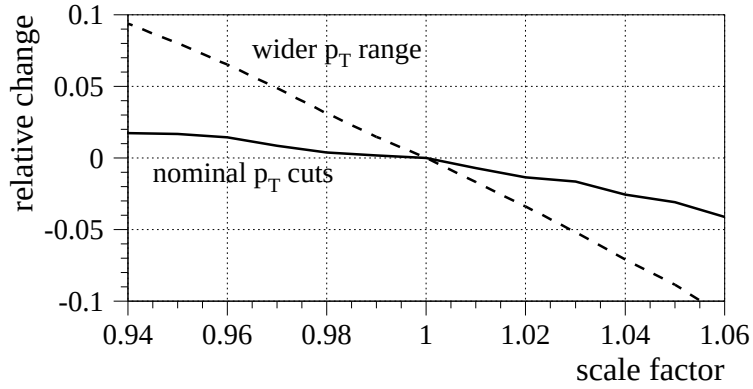

Figure 10: Relative variation of the ratio of efficiencies ($\epsilon_{\rm pk}/\epsilon_{\rm th}$) with an overall energy scale factor. The solid line shows a very small variation, given our nominal cuts on p_T, to be compared to a much larger variation if we had used looser p_T cuts meant to maximize the efficiency.

The efficiency for track reconstruction should be very high at an ILC detector. However, there is always an uncertainty in the value for that efficiency, which we took to be about 0.5%. We propagated this uncertainty to the cut on $N_{\rm tracks}$, since a random loss of tracks changes the shape of the distribution of $N_{\rm tracks}$. Since our cut is quite loose, however, the resulting uncertainty on the ratio of efficiencies is negligible.

Knowledge of the efficiency for charm jets for a given cut on $F_i^{(c)}$ is not easy to obtain. Based on the work described in ref. [26], we assumed an uncertainty of 0.5% on the charm efficiency. Although one might expect this uncertainty to be correlated between the two center-of-mass energies, we assumed no strong correlation and assign an uncertainty of 0.5% for the ratio of efficiencies.

The observable Y depends on the integrated luminosity at both center-of-mass energies. Traditionally, the luminosity is measured using Bhabha scattering, for which highly accurate theoretical cross-sections are available. The limiting systematic uncertainty for the LEP detectors comes from the acceptance of the luminosity calorimeters. Such an uncertainty would essentially cancel in the ratio of luminosities. Alternatively, one could define

JHEP09(2008)076

an effective luminosity through another clean QED process, such as $e^+e^- \to \mu^+\mu^-$, for which there is essentially no theoretical or experimental systematic effect. The precision of the ratio of luminosities would come from the statistical uncertainty on the number of $\mu^+\mu^-$ events recorded, which we estimate to be about 0.4%; this is the figure we use in this study.

Apart from instrumental issues such as the energy scale, track reconstruction efficiency, charm tagging efficiency and the measurement of the integrated luminosity, the estimate of the signal efficiency will depend on the modeling of the signal itself. While the production of a pair of stop quarks is well understood and can be modeled accurately, the non-perturbative aspects of the formation of stop hadrons which then decay into two or more jets are more problematic.[1] We have attempted to account for this fundamental difficulty by varying the parameter which controls the fragmentation function in our simulations. We used PYTHIA and the Peterson fragmentation function, with values of the fragmentation parameter reported by the OPAL Collaboration [28]. To be specific, we took $\epsilon_c = -0.031 \pm 0.011$ and $\epsilon_b = -0.0050 \pm 0.0015$, and propagated ϵ_b according to the assumption that $\epsilon_{\tilde{t}} = \epsilon_b\,(m_b/m_{\tilde{t}})^2$ [21, 29].

We varied ϵ_c and $\epsilon_{\tilde{t}}$ independently, and measured the efficiencies at the two center-of-mass energies. The impact of varying ϵ_c is small. For variations of the stop quark fragmentation, however, we find that the variation of the efficiencies is rather different, so the desired cancellation of systematic uncertainties is not achieved. In fact, most of the systematic uncertainty comes from the cut on p_T, and has an *opposite* sense at $\sqrt{s_{\rm th}}$ and $\sqrt{s_{\rm pk}}$.

The range in ϵ_b used in our simulations is quite broad. The more advanced measurements of b-quark fragmentation from ALEPH [30] and OPAL [31] give more constrained values: $\epsilon_b = -0.0031 \pm 0.0006$ (ALEPH) and $\epsilon_b = -0.0041 \pm 0.0004$ (OPAL), using rather different methodologies. On the basis of these measurements, one could argue that our assumed variation in ϵ_b is too large by a factor of two.

Rather than relying on LEP measurements to predict stop quark fragmentation, we investigated the potential of ILC data to constrain the fragmentation. We already noted that most of the sensitivity to stop quark fragmentation comes from the cut on p_T; however, the change in the shape of the p_T distribution is small. (The fact that the quantities chosen for cuts are insensitive to $\epsilon_{\tilde{t}}$ is a strong point of the analysis, of course.) We examined other kinematic quantities and found a few which exhibit clear changes in shape when we vary $\epsilon_{\tilde{t}}$. Four examples are shown in figure 11. The $M_{\rm vis}/\sqrt{s}$ distribution shows pronounced shifts as a function of $\epsilon_{\tilde{t}}$. Given an accumulation of a few $\times 10^4$ events at $\sqrt{s_{\rm pk}}$, one can show that the mean of this distribution alone would allow a differentiation of our three values $\epsilon_b = -0.0050 \pm 0.0015$ at more than ten sigma (statistical uncertainty only). If the energy scale uncertainty were a problem, then one could normalize $M_{\rm vis}$ to $E_{\rm vis}$ — a clear distinction between the three distributions is visible near the peak of $M_{\rm vis}/E_{\rm vis}$. The energy of the third jet, when it exists, shows a good sensitivity to $\epsilon_{\tilde{t}}$. (Recall that the jets are ordered in decreasing energy.) Better, perhaps, is the smaller of the two di-jet invariant masses formed by combining this third jet with the first and second jets. Although these considerations are not equivalent to a full study of a possible measurement of the stop fragmentation, they do

[1] Earlier analyses such as ref. [1] neglected this important problem.

JHEP09(2008)076

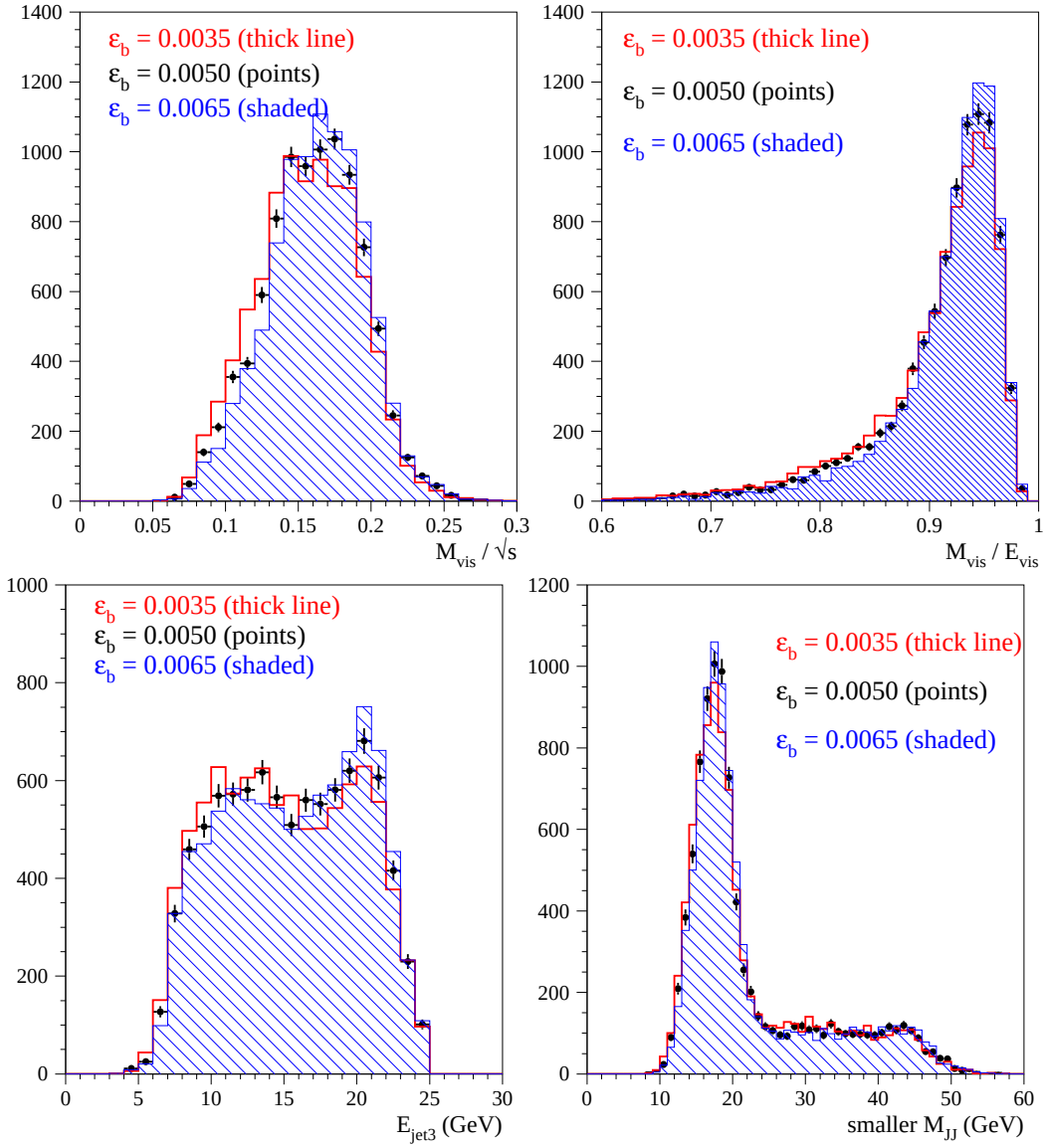

Figure 11: Changes in kinematic distributions at $\sqrt{s_{\rm pk}}$ for different assumed values of $\epsilon_{\tilde{t}}$, which are related directly to the listed values of ϵ_b through $\epsilon_{\tilde{t}} = \epsilon_b\,(m_b/m_{\tilde{t}})^2$. The solid points with error bars show the distribution with $\epsilon_b = -0.0050$, our default choice. The thick, unshaded red histogram shows $\epsilon_b = -0.0035$, and the thin, shaded blue histogram shows $\epsilon_b = -0.0065$.

indicate that a good measurement should be possible, well beyond the extrapolation of LEP results on ϵ_b to $\epsilon_{\tilde{t}}$ and all the attendant assumptions behind such an extrapolation. On this basis, we judge that the uncertainty on the stop fragmentation would be no larger than one-fourth of the uncertainty obtained by comparing simulations with $\epsilon_b = -0.0035$, -0.0050 and -0.0065, which corresponds to $\Delta\epsilon_{\tilde{t}} = (2.5 \times 10^{-6})/4 = 0.6 \times 10^{-6}$.

Another empirical quantity which induces an uncertainty on the selection efficiency is the mass of the neutralino, $m_{\tilde{\chi}_1^0}$. The mass difference $m_{\tilde{t}_1} - m_{\tilde{\chi}_1^0}$ clearly impacts the kinematic distributions, so the efficiency estimated from the simulation depends directly

JHEP09(2008)076

and strongly on $m_{\tilde{\chi}_1^0}$. We simulated a sample with $m_{\tilde{\chi}_1^0} = 108.2$ GeV, which is one GeV higher than our default value. The relative change in the selection efficiencies is roughly 10%. Since the changes are parallel, the ratio of efficiencies change by only 2.8%, once again illustrating the robustness of this method. Other studies have shown [3] that $m_{\tilde{\chi}_1^0}$ can be measured with an accuracy of 0.3 GeV or better, so we assign an uncertainty of 0.8% due to the unknown neutralino mass.

The predicted cross-sections depend on the beam energy and the beam energy spectrum. Due to beamstrahlung and other effects, the mean energy can be significantly lower than the peak value. While we used CIRCE for taking this fact into account, the question remains how well a program such as CIRCE can be validated using real data. This question has been addressed by several authors, using, for example, Bhabha scattering and radiative returns to the Z pole [32]. The studies indicate that models for the spectrum and the beam energy can be constrained directly from the data to an accuracy on the order of 0.1 GeV. We include this uncertainty as a direct uncertainty on $m_{\tilde{t}_1}$, but not on the observable Y.

Finally, we must consider uncertainties on the estimated contributions from background processes. The SM backgrounds fall naturally in two categories: two-photon interactions, which are difficult to predict, and the others, which involve high-p_T electro-weak processes, for which direct theoretical calculations are reliable. We also consider background contributions from the production of other supersymmetric particles.

Two-photon interactions cannot be fully described by perturbative QCD, and so phenomenological models are required [33]. These must be tuned to match real data, which is difficult due to the fact that most two-photon scattering events emit particles that are lost down the beam pipe. Parameters pertaining to the softest interactions are difficult to constrain; fortunately, such interactions are easily eliminated by our cuts on p_T, N_{tracks} and E_{vis}. Many of the events coming in at higher p_T can be described using models with a basis in perturbative QCD. The investigations of the photon structure functions by the LEP Collaborations illustrate the procedure of tuning parameters and confronting the models with real data, leading to interesting conclusions about the success of the various models [34 – 36]. It is not straightforward to translate those conclusions into constraints on our two-photon background, although figures 19, 21 and 23 in the report from the LEP Working Group [36] and figures in the OPAL papers [35] are quite relevant for our study, and indicate that modeling the tails of the p_T distribution at the 20% level should be possible. Assuming that the study of two-photon interactions would be greatly extended at the ILC, we assign a 20% uncertainty to the background estimate for two-photon interactions. The resulting relative uncertainty on the Y observable is 0.8%.

The dominant background is $e^+e^- \to We\nu$, according to table 4 (and table 6). A precise prediction of this background requires accurate measurements of this process combined with the calculation of higher-order radiative corrections. While a complete NLO calculation of that process is missing, a recent result for the related process of W pair production [37] suggests that a NLO calculation of $We\nu$ is feasible within the next years with an error remaining well below 0.5%. The impact on Y is negligible, on the order of 0.1%, relative.

A summary of the experimental systematic uncertainties for the sequential-cut analysis is shown in table 7. A good cancellation of experimental systematics is obtained, except

JHEP09(2008)076

variable	error on variable	relative shift in expected signal yield (%) $\sqrt{s_{\rm th}} = 260$ GeV	$\sqrt{s_{\rm pk}} = 500$ GeV	error on Y (%)
energy scale	1%	3.7	3.1	0.6
tracking efficiency	0.5%	negligible		
charm tagging efficiency	0.5%	taken to be 0.5		
luminosity	-	0.4	0.2	0.4
charm fragmentation	0.011	0.3	0.8	0.6
stop fragmentation	0.6×10^{-6}	0.6	0.2	0.7
neutralino mass	0.3 GeV	3.8	3.0	0.8
background estimate	-	0.8	0.1	0.8

Table 7: Evaluation of experimental uncertainties on Y, for the sequential-cut analysis. The last column gives the relative uncertainty on Y.

for the stop quark fragmentation uncertainty and the background estimation. The goal of the new method is therefore fairly well achieved with this set of sequential cuts. The implications for the measurement of the observable Y and the inferred mass $m_{\tilde{t}_1}$ are discussed in section 6.

4.2 Systematics for the iterative discriminant analysis

We evaluated the impact of the sources of systematics listed on page 18 in a manner similar to the methods of section 4.1. We scaled all kinematic inputs to the IDA according to an overall energy scale uncertainty. The systematic uncertainty from the number of tracks is assumed to be negligible. The variations in the charm and stop quark fragmentation functions were evaluated as before. The sensitivity to $m_{\tilde{\chi}_1^0}$ and the uncertainty on the background estimate were evaluated precisely as above. The luminosity uncertainty is, of course, the same as in the sequential-cut analysis.

The resulting systematic uncertainties are listed in table 8. We observe a much larger uncertainty coming from the scale uncertainty as compared to the sequential-cut analysis (see table 7). With multi-variate methods such as the IDA, it is difficult to ascertain what role any given quantity plays in the final output variable, so no dissection of the IDA to reveal the sensitivities to the energy scale is possible. Furthermore, one cannot tune the operation of the IDA in order to balance efficiencies for each quantity, as we did for thrust T and event-p_T in the sequential-cut analysis. For this kind of precision measurement, it may appear that the better discrimination of signal and background provided by the IDA as implemented here is of limited value in light of the larger and uncontrollable sensitivity to experimental sources of systematic uncertainty. However, it might be possible to extend the IDA to take into account systematic errors in the optimization. We have not attempted to design such an analysis for this work. In any case, when performing a measurement with real data, one would welcome an alternative analysis in order to check the robustness and stability of the measurement.

JHEP09(2008)076

variable	error on variable	relative shift in expected signal yield (%) $\sqrt{s_{\rm th}} = 260$ GeV	$\sqrt{s_{\rm pk}} = 500$ GeV	error on Y (%)
energy scale	1%	3.4	1.3	2.3
tracking efficiency	0.5%	negligible		
charm tagging efficiency	0.5%	taken to be 0.5		
luminosity	-	0.4	0.2	0.4
charm fragmentation	0.011	0.1	0.6	0.5
stop fragmentation	0.6×10^{-6}	0.1	0.8	0.7
neutralino mass	0.3 GeV	3.7	1.6	2.2
background estimate	-	0.3	0.2	0.1

Table 8: Evaluation of experimental uncertainties on Y, for the IDA. The last column gives the relative uncertainty on Y.

In section 6.4, we show the power of the IDA in the discovery of a light stop quark.

5. Theoretical uncertainties

The inference of the stop mass from stop cross-section measurements requires precise theoretical calculations for the cross-sections. The stop production cross-section receives large corrections in particular from QCD gluon exchange between the final state stops. Near threshold, when the stop quarks are slowly moving, these effects become very large, which is the well-known Coulomb correction [38]. The NLO QCD corrections to stop production have been computed several years ago [15] and it was found that the corrections range between about 10% at high energies and up to 100% near threshold. This shows that higher-order corrections are crucial.

Over the last few years, sophisticated techniques have been developed for calculating top-pair production at NNLO [39]. Near threshold, they include resummation of terms of order $O(\alpha_{\rm s}/v)$ for the low velocity v of the top-quarks. For the production of scalar quarks, similar calculations are not yet done. However, one can use partial results to obtain a reliable estimate of the uncertainty of the NNLO corrections. At NNLO order, several contributions enter in the computation. The largest effect near threshold arises from the Coulomb correction. The impact of the Coulomb corrections is calculated through NNLO order [40], including resummation via non-relativistic QCD. Technically, here the non-relativistic Schrödinger equation is used for computing the Coulomb effects [41].

Similar to the case of top pair production, it is found that the NNLO term to stop pair production is of similar order of magnitude as the NLO term, i.e., the perturbation series is converging rather slowly. From the behavior of the perturbation series and the remaining scale dependence, the size of the missing higher-order contributions is estimated to be around 7% at 260 GeV and 2.5% at 500 GeV.

JHEP09(2008)076

However, we want to point out that several improvements to this straightforward approach could be made. Besides the large Coulomb-type corrections of order $O(\alpha_s/v)$, there are also potentially large logarithmic contributions $O(\log(\alpha_s/v))$. They can be resummed with more sophisticated techniques, for instance velocity non-relativistic QCD [42] or potential non-relativistic QCD [43]. Using the results of ref. [44] for the NLO corrections to squark pair production, it is found that the uncertainty with respect to the NLO computation is reduced significantly. A similar improvement can be expected at the NNLO level. In addition, instead of directly computing the total cross-section near threshold, one can describe it through moments [45] that avoid the non-perturbative contribution of stoponium bound states that can form just below the nominal stop-pair threshold. With these refinements it is expected that the theoretical uncertainty can be brought down by a factor of two (however the actual calculation remains for the future). So here an uncertainty of 3.5% at 260 GeV and 1% at 500 GeV are assumed.

Besides the QCD corrections, the electroweak corrections need to be considered. The NLO electroweak corrections have been computed [46], and found to amount to several per-cent. While they need to be taken into account, the NNLO corrections are expected to be much less than 1%, with the exception of leading initial- and final-state QED corrections that can easily be resummed to higher orders.

Combining the two errors, a total theoretical error of 4% at 260 GeV and 1.5% at 500 GeV can be assigned. Pessimistically, we add these two uncertainties linearly, and assign a theoretical uncertainty of 5.5% for the quantity Y.

6. Results and implications

We derive the expected measurement error on the stop quark mass and discuss the implications for particle physics predictions of the relic density of dark matter. We also discuss the luminosity needed to discover a light stop quark in this scenario, using the IDA method.

6.1 Precision on the stop quark mass

A final assessment of the achievable precision on the stop mass will be based on the statistical and all systematic uncertainties. Table 9 summarizes these uncertainties for the observable Y defined by eq. (2.3). One sees that the IDA method achieves a smaller statistical uncertainty on Y at the cost of a larger experimental systematic uncertainty. It would be important, in a measurement with real data, to implement two methods as we have done here, and check the consistency of the results.

The stop quark mass is inferred from the measured values of the observable Y following the example described in section 2. The differing efficiencies for the sequential-cut and IDA methods lead to different central values for Y and for the slope dY/dM at that point. The inferred uncertainties on the stop quark mass are summarized in table 10 and are similar for the two analyses. We conclude that the stop quark mass could be measured with an uncertainty of $\Delta m_{\tilde{t}_1} = 0.42$ GeV.

We investigated the dependence of the measurement error on the integrated luminosity. There is very little change in the statistical uncertainty if we increase the luminosity

JHEP09(2008)076

error source for Y	sequential cuts	IDA method
detector effects	0.9	2.4
charm fragmentation	0.6	0.5
stop fragmentation	0.7	0.7
neutralino mass	0.8	2.2
background contribution	0.8	0.1
sum of experimental systematics	1.7	3.4
statistical	3.1	2.7
sum of experimental errors	3.5	4.3
theory for signal cross-section	5.5	5.5
total error ΔY	6.5	7.0

Table 9: Summary of relative statistical and systematic uncertainties (in percent) on the observable Y.

on peak, but the variation with the luminosity at $\sqrt{s_{\rm th}} = 260$ GeV is interesting — see figure 12. The experimental uncertainty is dominated by the statistical contribution, so a decrease in the luminosity from our assumed value of $\mathcal{L}_{\rm th} = 50$ fb^{-1} has a significant impact. On the other hand, the theoretical uncertainty is very large by comparison, so increasing $\mathcal{L}_{\rm th}$ hardly improves the total error on $m_{\tilde{t}_1}$. A luminosity in the range 30 fb$^{-1} < \mathcal{L}_{\rm th} < 80$ fb^{-1} would appear to be optimal, for this analysis.

The dominant uncertainty comes from the theoretical calculation of the signal cross-section. As discussed in section 5, this uncertainty comes mainly from higher-order corrections which are not easily summed at threshold. The estimate of this theory error relies on present computational techniques and some expectations on how they might improve in the future. However, the progress in calculations of radiative corrections can not really be predicted, so the assumed value for the theoretical uncertainty at the time when ILC is running might well be somewhat different than the value reported in table 9. In particular, history has shown that people working on loop computations often overcame big problems with unexpected ingenuity, in order to be able to make most of precise measurements. Therefore, in the following, the combined error in table 9 will be taken as a conservative estimate. If one were to set aside the theoretical error on the cross section, then the total experimental error is quite small, amounting to 3.5%–4.3% on Y. In this case, the error on the stop quark mass would be a little larger than $\Delta m_{\tilde{t}_1} = 0.2$ GeV.

6.2 Comparison with previous results

A previous study investigated the potential of the ILC running at $\sqrt{s} = 500\,\text{GeV}$ to discover a light stop quark and measure its parameters [1]. The theoretical scenario addressed is the same as the one we have studied in this paper. It was assumed that 250 fb^{-1} would be taken at two beam polarization combinations: $P(e^-)/P(e^+) = +80\%/-60\%$ and $-80\%/+60\%$. Measurements of the stop squark production cross sections at these two

error category	measurement error $\Delta m_{\tilde{t}_1}$ (GeV)	
	sequential cuts	IDA method
statistical	0.19	0.17
sum of experimental systematics on Y	0.10	0.21
beam spectrum and calibration	0.1	0.1
sum of experimental errors	0.24	0.28
sum of all experimental and theoretical errors	0.42	0.44

Table 10: Estimated measurement errors (in GeV) on the stop quark mass

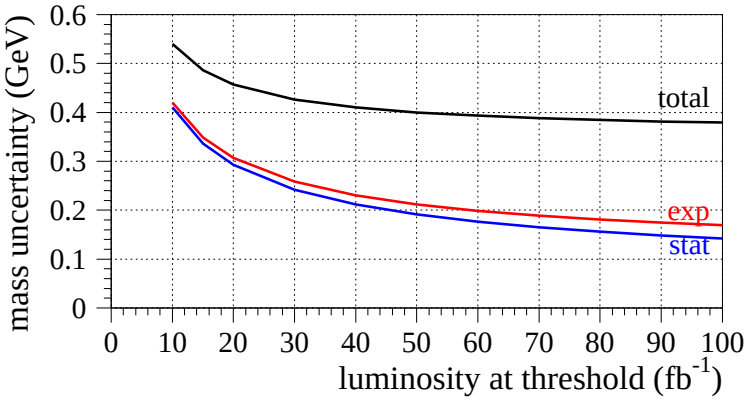

Figure 12: Decrease of the statistical uncertainty (blue line), total experimental uncertainty (red line) and total uncertainty on $m_{\tilde{t}_1}$ (black line), as a function of the integrated luminosity $\mathcal{L}_{\rm th}$ at $\sqrt{s_{\rm th}}$.

polarizations are sufficient to deduce the mixing angle and mass of the stop squark. A host of systematic uncertainties was considered, with the conclusions that the *absolute* cross-sections could be measured to 1.3%–2.4%, dominated by experimental systematic uncertainties (the statistical uncertainty was 0.8%). Under the given theoretical scenario, the total error on the stop quark mass was estimated[2] to be $\Delta m_{\tilde{t}_1} = 1.2\,\text{GeV}$.

Our theoretical scenario coincides with the one studied in ref. [1], and the method proposed here leads to a total error on the stop quark mass that is more than two times smaller: $\Delta m_{\tilde{t}_1} = 0.42\,\text{GeV}$, even though a much smaller integrated luminosity is assumed (specifically, $50+250\ \text{fb}^{-1}$ compared to $2\times 250\ \text{fb}^{-1}$). This improvement is quite helpful for the calculation of the relic density, as discussed in the next section. We would like to point out, however, that the basis for the experimental analysis in ref. [1] differs significantly from what was used for the present analysis. In particular, the fragmentation of the stop squark and of the charm quark produced in its decay was not simulated in ref. [1], leading to very different signal characteristics which are not realistic.

[2]Note that the error of 1.2 GeV is slightly larger than reported in eq. (17) in ref. [1], since we are using the scenario from ref. [3] with large slepton masses, leading to a larger neutralino mass error, which in turn increases the stop mass uncertainty.

JHEP09(2008)076

We re-evaluated the mass measurement method of ref. [1], making no attempt to re-optimize the cuts given there. We used the simulated data and sequential cuts from the present study, as explained in section 3, which properly take into account fragmentation effects. We also included the estimates for systematic errors from sections 4 (table 7) and 5. Taking into account correlations between the systematic errors for the two cross section measurements for $P(e^-)/P(e^+) = +80\%/-60\%$ and $-80\%/+60\%$, we find that $\Delta m_{\tilde{t}_1} \approx 5\,\mathrm{GeV}$. The error is dominated by the systematic uncertainties due to the energy scale and the neutralino mass. While it is likely that these uncertainties can be reduced by optimizing the cuts for this method, it is clear that the uncertainty on the stop quark mass, $\Delta m_{\tilde{t}_1} = 1.2$ GeV, reported in ref. [1] was substantially underestimated, so that our present result $\Delta m_{\tilde{t}_1} = 0.42\,\mathrm{GeV}$ represents a major step forward.

6.3 Implications for relic density calculation

Precise measurements of supersymmetric particle properties at the LHC and ILC can be used to compute the dark matter relic abundance so as to compare with cosmological observations. If stop-neutralino co-annihilation is relevant, as in the scenario studied here [3], it is important to measure the stop-neutralino mass difference very precisely. The extraction of the neutralino properties, in particular the lightest neutralino mass, is studied in detail in ref. [3]. It is found that a high precision of $\Delta m_{\tilde{\chi}_1^0} \approx 0.3\,\mathrm{GeV}$ for the lightest neutralino mass can be achieved at the ILC, and also the other neutralino parameter can be inferred rather well.

The limiting factor in the accuracy of the dark matter estimation is therefore the precision of the measurement of the scalar top quark mass. As discussed in the previous section, an older study using cross-section measurements at $\sqrt{s} = 500\,\mathrm{GeV}$ found $\Delta m_{\tilde{t}_1} = 1.2\,\mathrm{GeV}$ and $|\cos\theta_{\tilde{t}}| < 0.077$ for the stop mass and mixing angle [1, 3]. Based on these expected experimental results, the relic dark matter density is computed with the codes described in ref. [11, 47]. Figure 13 shows the result of a scan over the MSSM parameter space. The scattered gray dots indicate the region allowed by the collider experimental uncertainty, as a function of the measured stop mass. The horizontal bands depict the relic density as measured by WMAP [5] with one and two standard deviation errors. Here, Ω_{CDM} is the ratio of the dark matter energy density to the critical density $\rho_c = 2H_0^2/(8\pi G_{\mathrm{N}})$, with the Hubble constant $H_0 = h \times 100$ km/s/Mpc and Newton's constant G_{N}. At the 1σ level, the astrophysical observations lead to $0.103 < \Omega_{\mathrm{CDM}} h^2 < 0.116$. With a stop mass measurement error of $m_{\tilde{t}_1} = (122.5 \pm 1.2)$ GeV, the relic density can be predicted to $0.082 < \Omega_{\mathrm{CDM}} h^2 < 0.139$ at the 1σ level. With the new result of this work, $\Delta m_{\tilde{t}_1} = 0.42$ GeV, the relic density can be computed much more precisely, yielding the result $0.096 < \Omega_{\mathrm{CDM}} h^2 < 0.124$. This precision is very comparable to the direct WMAP measurement,[3] as indicated by the black dots in figure 13.

As pointed out above, the estimate of a stop mass error of $\Delta m_{\tilde{t}_1} = 0.42$ GeV is based on a rather conservative evaluation of systematic errors. In particular, this value is dominated

[3]The PLANCK mission is expected to improve the WMAP measurement substantially; the study described here cannot match the precision expected from PLANCK [48].

JHEP09(2008)076

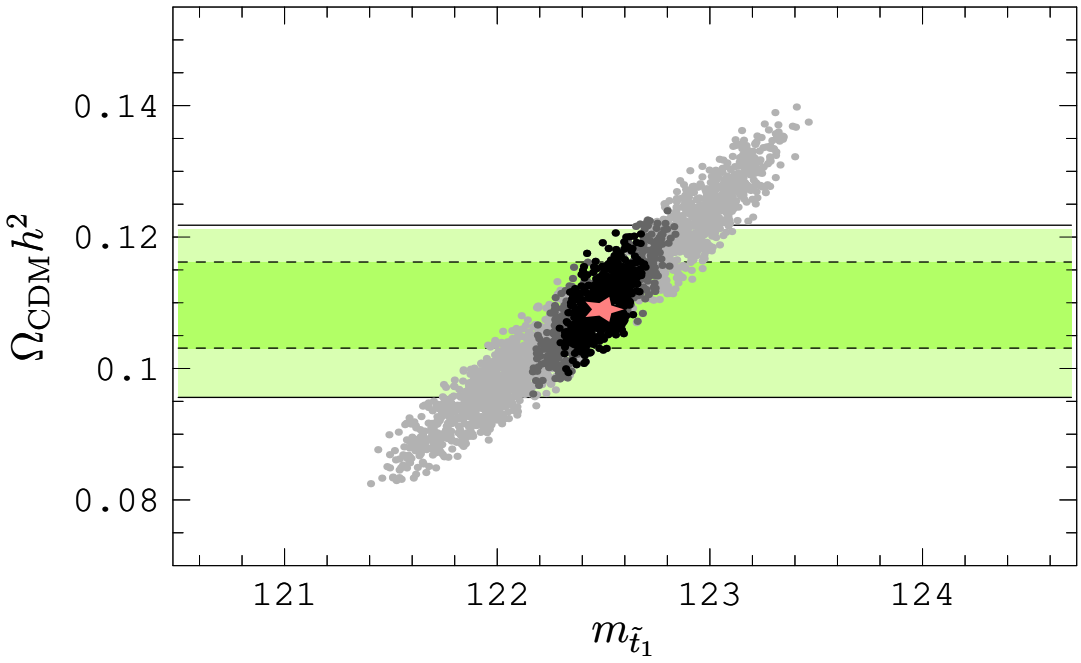

Figure 13: Computation of dark matter relic abundance $\Omega_{\rm CDM}h^2$ taking into account estimated experimental errors for stop, chargino, neutralino and Higgs sector measurements at future colliders. The dots correspond to a scan over the 1σ ($\Delta\chi^2 \leq 1$) region allowed by the experimental errors, as a function of the measured stop mass, for a mass measurement error of 1.2 GeV (light gray dots), 0.42 GeV (dark gray dots) and 0.24 GeV (black dots). The underlying scenario used as input is indicated by the red (light) star. The horizontal shaded bands show the 1σ and 2σ constraints on the relic density measured by WMAP.

by the conjectured theory error on the prediction of signal and background cross-sections. If on the other hand, with progress in calculation methods, the theory error could be reduced to a sub-dominant level, the remaining statistical and systematic experimental errors would give a stop mass error of $\Delta m_{\tilde{t}_1} = 0.24$ GeV for the cut-based analysis and $\Delta m_{\tilde{t}_1} = 0.28$ GeV for the IDA. The amelioration of the prediction for the dark matter relic density due to this improvement in stop mass precision is illustrated in figure 13.

For this accuracy of the stop mass measurement, the uncertainty of the dark matter prediction becomes limited due to the expected experimental errors in the lightest neutralino mass and mixing angles, which we have taken from ref. [3]. As a result, taking an error of $\Delta m_{\tilde{t}_1} = 0.24$ GeV for the stop mass, we find $0.099 < \Omega_{\rm CDM}h^2 < 0.121$, which is only a small improvement in the precision of the dark matter density prediction with respect to $\Delta m_{\tilde{t}_1} = 0.42$ GeV.

6.4 Discovery of the light stop quark

The main focus of this paper is the measurement of the stop quark mass. It is interesting, nonetheless, to consider the utility of these selections for discovering the light stop quark

JHEP09(2008)076

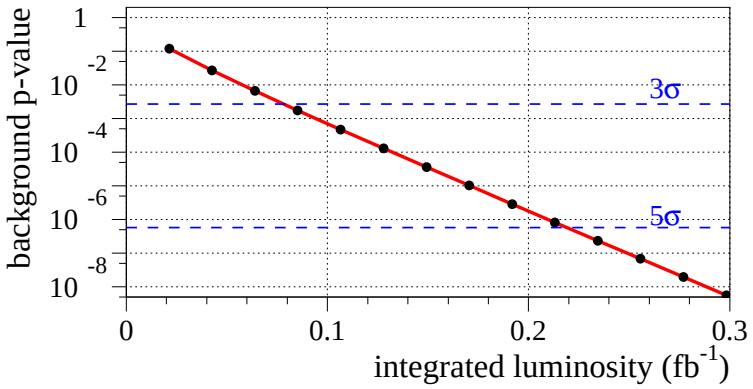

Figure 14: p-values as a function of integrated luminosity $\mathcal{L}$. The black dots on the line show hypothetical integral numbers of observed events, starting at $N = 1$ for $\mathcal{L} = 0.02$ fb^{-1}.

at the ILC. The IDA-based selection, in particular, achieves a very low background and a high efficiency – see table 6 in Subsection 3.3.

We examined this issue assuming that the ILC collects data at $\sqrt{s_{\rm pk}} = 500\,\text{GeV}$, with *unpolarized* beams, as one might expect at start-up. The signal cross-section for this scenario is $\sigma_{\tilde{t}} = 118\,\text{fb}$. The nominal IDA selection efficiency is $\epsilon = 0.416$ and the background cross-section for unpolarized beams is $\sigma_b = 10.3\,\text{fb}$. Tightening the selection to reduce the background improves the sensitivity of the analysis only very slightly. This information allows a calculation of the expected tail probability or p-value as a function of integrated luminosity, $\mathcal{L}$. Specifically, we computed the p-value setting the hypothetical number of observed events equal to the mean of the corresponding Poisson distributions (signal and background), as a function of $\mathcal{L}$. The result is shown in figure 14 by the thick red line. The black dots on the line show hypothetical integral numbers of observed events, starting at $N = 1$ for $\mathcal{L} = 0.02$ fb^{-1}. The plot clearly indicates that a luminosity of only $\mathcal{L} \approx 240$ pb^{-1} would produce eleven observed events, on average, and the significance of ten signal events over the expected background would be more than 5σ. The uncertainty on the background estimate and the signal efficiency have a negligible impact on this result.

This example applies only to our given scenario, with $m_{\tilde{t}_1} = 122.5$ GeV, $m_{\tilde{\chi}_1^0} = 107.2$ GeV and $\cos\theta_{\tilde{t}} = 0.01$. Further investigations would be needed in order to understand how well this IDA selection would perform for other mass and mixing combinations.

7. Summary

A new method for a precise measurement of the stop quark mass has been described, based on the ratio of yields at the peak stop quark pair production cross section, and near threshold. This ratio is far less sensitive to experimental uncertainties than other methods, leading to a very low estimated uncertainty, still dominated by the statistical uncertainty and the theoretical uncertainty (which is also present for other methods based on a cross-section measurement). We studied a specific scenario in detail, with an emphasis on analysis techniques and systematic uncertainties. We placed special emphasis on the modeling of the stop quark and charm fragmentation uncertainties, and suggest how fragmentation models

JHEP09(2008)076

could be constrained with data taken at the ILC. Previous studies had not considered this source of uncertainty. This method is general, and could be applied to other species, provided an accurate prediction for the excitation curve is or can be available. For weakly interacting particles, such as staus, the theoretical uncertainty is much smaller and the advantage of the new method would be even more impressive.

An important part of our studies is the use of multi-variate methods to isolate a very clean stop quark signal. For this we utilize the Iterative Discriminant Analysis (IDA) used previously at LEP. It is interesting that a carefully-tuned set of sequential cuts achieves a much smaller systematic uncertainty, and hence a better overall result for the stop quark mass measurement in this method. The superior background rejection of the IDA, however, is extremely useful when searching for a stop signal, and we give an illustration for $\sqrt{s} =$ 500 GeV, which shows that a five-sigma significance could be obtained by the IDA selection with only 240 pb^{-1}.

The reduction of the uncertainty on the stop mass from about $\Delta m_{\tilde{t}_1} = 1.2$ GeV in ref. [1, 3] to $\Delta m_{\tilde{t}_1} = 0.42$ GeV in this analysis is crucial for testing theoretical explanations of the dark matter relic density in the light-stop co-annihilation scenario. With these new results, the theoretical calculation has an accuracy equal to the two-sigma uncertainty of the WMAP measurements. The remaining uncertainty is no longer dominated by $\Delta m_{\tilde{t}_1}$.

Acknowledgments

The authors are grateful to A. Kraan, T. Kuhl and S. Mrenna for useful discussions and expert advice on Pythia and Simdet. C.M. wants also to thank particularly M. Demarteau, H. Fisk, R. Rubinstein and J. Strait of Fermilab for their support. A.S. would like to thank A. Finch, H. Nowak and colleagues from LCFI Collaboration for discussions, and STFC and Lancaster University for partially funding the project.

ANL is supported by the U.S. Department of Energy (DoE) under Contract DE-AC02-06CH11357. Fermilab is operated by Fermi Research Alliance, LLC under Contract DE-AC02-07CH11359 with the U.S. Department of Energy. The research effort by M.S. is supported by DoE Contract DE-FG02-91ER40684.

References

[1] M.S. Carena et al., *Analyzing the scalar top co-annihilation region at the ILC*, *Phys. Rev.* **D 72** (2005) 115008 [hep-ph/0508152].

[2] C. Milsténe et al., *Analysis of stops with small stop — neutralino mass difference at a LC*, in *Proceedings of International Workshop on Linear Colliders (LCWS* 2005*), Stanford California March* 18–22 2005 [hep-ph/0508154];
A. Sopczak et al., *Scalar top quark studies with various visible energies*, hep-ph/0605225;
C. Milsténe, M. Carena, A. Finch, A. Freitas, H. Nowak and A. Sopczak, *The light stop quark with small stop-neutralino difference in the MSSM*, in *Proceedings of International Linear Collider Physics and Detector Workshop, Snowmass Colorado U.S.A. August* 14-27 2005, *eConf* **C0508141** (2005) ALCPG0317;

A. Finch, H. Nowak and A. Sopczak, *Determination of the scalar top mass at a linear e^+e^- collider*, in *Proceedings of the International Conference on Linear Colliders (LCWS* 04*), Paris France April* 19–24 2004;
H. Nowak, A. Finch and A. Sopczak, *Analysis of stops with small stop-neutralino mass difference at a LC*, in *Proceedings of the International Linear Collider Workshop (LCWS* 05*), Stanford California U.S.A. March* 18–22 2005, *eConf* **C050318** (2005) 0219;
A. Finch, A. Sopczak and H. Nowak, *A scalar top study with c-quark tagging at a linear e^+e^- collider*, contributed paper EPS370, *International Europhysics Conference on High-Energy Physics (HEP* 2003*), Aachen Germany July* 17–23 2003, LC-PHSM-2003-075;
A. Bartl et al., *Search of stop, sbottom, tau-sneutrino and stau at an e^+e^- linear collider with $\sqrt{s} = 0.5$ TeV to 2 TeV*, *Z. Physik* **C 76** (1997) 549 [hep-ph/9701336];
A. Finch, H. Nowak and A. Sopczak, *Precision measurements in the scalar top sector of the MSSM at a linear e^+e^- collider*, hep-ph/0211140;
A. Bartl, S. Hesselbach, K. Hidaka, T. Kernreiter and W. Porod, *Impact of SUSY CP phases on stop and sbottom decays in the MSSM*, hep-ph/0306281.

[3] M.S. Carena and A. Freitas, *Collider searches and cosmology in the MSSM with heavy scalars*, *Phys. Rev.* **D 74** (2006) 095004 [hep-ph/0608255].

[4] T.G.M. Malmgren and K.E. Johansson, *An iterative discriminant analysis method to search for the Higgs particle at LEP-2*, *Nucl. Instrum. Meth.* **A403** (1998) 481.

[5] WMAP collaboration, D.N. Spergel et al., *Wilkinson Microwave Anisotropy Probe (WMAP) three year results: implications for cosmology*, *Astrophys. J. Suppl.* **170** (2007) 377 [astro-ph/0603449].

[6] SDSS collaboration, M. Tegmark et al., *The 3D power spectrum of galaxies from the SDSS*, *Astrophys. J.* **606** (2004) 702 [astro-ph/0310725].

[7] M.S. Carena, M. Quirós and C.E.M. Wagner, *Opening the window for electroweak baryogenesis*, *Phys. Lett.* **B 380** (1996) 81 [hep-ph/9603420].

[8] M. Laine, *Effective theories of MSSM at high temperature*, *Nucl. Phys.* **B 481** (1996) 43 [*Erratum ibid.* **B 548** (1999) 637] [hep-ph/9605283];
M. Losada, *High temperature dimensional reduction of the MSSM and other multi-scalar models*, *Phys. Rev.* **D 56** (1997) 2893 [hep-ph/9605266];
G.R. Farrar and M. Losada, *SUSY and the electroweak phase transition*, *Phys. Lett.* **B 406** (1997) 60 [hep-ph/9612346];
B. de Carlos and J.R. Espinosa, *The baryogenesis window in the MSSM*, *Nucl. Phys.* **B 503** (1997) 24 [hep-ph/9703212];
D. Bödeker, P. John, M. Laine and M.G. Schmidt, *The 2-loop MSSM finite temperature effective potential with stop condensation*, *Nucl. Phys.* **B 497** (1997) 387 [hep-ph/9612364].

[9] M.S. Carena, M. Quirós and C.E.M. Wagner, *Electroweak baryogenesis and Higgs and stop searches at LEP and the Tevatron*, *Nucl. Phys.* **B 524** (1998) 3 [hep-ph/9710401].

[10] M. Laine and K. Rummukainen, *The MSSM electroweak phase transition on the lattice*, *Nucl. Phys.* **B 535** (1998) 423 [hep-lat/9804019];
M. Losada, *The two-loop finite-temperature effective potential of the MSSM and baryogenesis*, *Nucl. Phys.* **B 537** (1999) 3 [hep-ph/9806519]; *Mixing effects in the finite-temperature effective potential of the MSSM with a light stop*, *Nucl. Phys.* **B 569** (2000) 125 [hep-ph/9905441];

JHEP09(2008)076

M. Laine and M. Losada, *Two-loop dimensional reduction and effective potential without temperature expansions*, *Nucl. Phys.* **B 582** (2000) 277 [hep-ph/0003111];
M. Laine and K. Rummukainen, *Two Higgs doublet dynamics at the electroweak phase transition: a non-perturbative study*, *Nucl. Phys.* **B 597** (2001) 23 [hep-lat/0009025].

[11] C. Balázs, M.S. Carena and C.E.M. Wagner, *Dark matter, light stops and electroweak baryogenesis*, *Phys. Rev.* **D 70** (2004) 015007 [hep-ph/0403224].

[12] J.K. Mizukoshi, H. Baer, A.S. Belyaev and X. Tata, *Sneutrino mass measurements at e^+e^- linear colliders*, *Phys. Rev.* **D 64** (2001) 115017 [hep-ph/0107216].

[13] D. Asner et al., *Higgs physics with a gamma gamma collider based on CLIC* 1, *Eur. Phys. J.* **C 28** (2003) 27 [hep-ex/0111056].

[14] G.J. Feldman and R.D. Cousins, *A unified approach to the classical statistical analysis of small signals*, *Phys. Rev.* **D 57** (1998) 3873 [physics/9711021].

[15] H. Eberl, A. Bartl and W. Majerotto, *SUSY-QCD corrections to scalar quark pair production in e^+e^- annihilation*, *Nucl. Phys.* **B 472** (1996) 481 [hep-ph/9603206].

[16] T. Sjöstrand et al., *High-energy-physics event generation with PYTHIA* 6.1, *Comput. Phys. Commun.* **135** (2001) 238 [hep-ph/0010017];
T. Sjöstrand, L. Lönnblad and S. Mrenna, *PYTHIA* 6.2*: physics and manual*, hep-ph/0108264.

[17] A. Freitas, D.J. Miller and P.M. Zerwas, *Pair production of smuons and selectrons near threshold in e^+e^- collisions*, *Eur. Phys. J.* **C 21** (2001) 361 [hep-ph/0106198];
A. Freitas, A. von Manteuffel and P.M. Zerwas, *Slepton production at e^+e^- and e^-e^- linear colliders*, *Eur. Phys. J.* **C 34** (2004) 487 [hep-ph/0310182].

[18] F. Yuasa et al., *Automatic computation of cross sections in HEP: status of GRACE system*, *Prog. Theor. Phys. Suppl.* **138** (2000) 18 [hep-ph/0007053].

[19] CompHEP collaboration, E. Boos et al., *CompHEP* 4.4*: automatic computations from Lagrangians to events*, *Nucl. Instrum. Meth.* **A534** (2004) 250 [hep-ph/0403113].

[20] T. Ohl, *CIRCE version* 1.0*: beam spectra for simulating linear collider physics*, *Comput. Phys. Commun.* **101** (1997) 269 [hep-ph/9607454].

[21] C. Peterson, D. Schlatter, I. Schmitt and P.M. Zerwas, *Scaling violations in inclusive e^+e^- annihilation spectra*, *Phys. Rev.* **D 27** (1983) 105.

[22] T. Sjöstrand, *Program to turn gluinos into gluino-hadrons*, http://www.thep.lu.se/∼torbjorn/pythia/main73.f.

[23] A.C. Kraan, *Interactions of heavy stable hadronizing particles*, *Eur. Phys. J.* **C 37** (2004) 91 [hep-ex/0404001].

[24] M. Pohl and H.J. Schreiber, *SIMDET - Version 4: a parametric Monte Carlo for a TESLA detector*, hep-ex/0206009.

[25] T. Kuhl, *N-tuple working on Simdet DST structure*, http://www.desy.de/∼kuhl/ntuple/ntuple.html.

[26] T. Kuhl, *Hadronic branching ratio of a SM-like Higgs boson at a future linerar collider*, in *Proceedings of the International Conference on Linear Colliders (LCWS* 04*), Paris France April* 19–24 2004; *Vertex detector as a physics tool for TESLA*, *Nucl. Instrum. Meth.* **A511** (2003) 221.

JHEP09(2008)076

[27] L3 collaboration, M. Acciarri et al., *Study of Z boson pair production in e^+e^- interactions at $\sqrt{s} = 192\ GeV$ – $202\ GeV$*, *Phys. Lett.* **B 497** (2001) 23 [hep-ex/0010004];
OPAL collaboration, G. Abbiendi et al., *Study of Z pair production and anomalous couplings in e^+e^- collisions at $\sqrt{s}$ between $190\ GeV$ and $209\ GeV$*, *Eur. Phys. J.* **C 32** (2003) 303 [hep-ex/0310013].

[28] OPAL collaboration, G. Alexander et al., *A comparison of b and (u d s) quark jets to gluon jets*, *Z. Physik* **C 69** (1996) 543.

[29] OPAL collaboration, K. Ackerstaff et al., *Search for scalar top and scalar bottom quarks at $\sqrt{s} = 183\ GeV$ at LEP*, *Eur. Phys. J.* **C 6** (1999) 225 [hep-ex/9808026].

[30] ALEPH collaboration, A. Heister et al., *Study of the fragmentation of b quarks into B mesons at the Z peak*, *Phys. Lett.* **B 512** (2001) 30 [hep-ex/0106051].

[31] OPAL collaboration, G. Abbiendi et al., *Inclusive analysis of the b quark fragmentation function in Z decays at LEP*, *Eur. Phys. J.* **C 29** (2003) 463 [hep-ex/0210031].

[32] K. Mönig, *Measurement of the differential luminosity using Bhabha events in the forward-tracking region at TESLA*, LC-PHSM-2000-060;
G. Wilson, *Precision measurement of the W mass with a polarised threshold scan at a linear collider*, LC-PHSM-2001-009.

[33] M. Krawczyk, A. Zembrzuski and M. Staszel, *Survey of present data on photon structure functions and resolved photon processes*, *Phys. Rept.* **345** (2001) 265 [hep-ph/0011083];
S. Soldner-Rembold, *Photon structure*, hep-ex/0010012.

[34] L3 collaboration, M. Acciarri et al., *Measurement of the photon structure function at high Q^2 at LEP*, *Phys. Lett.* **B 483** (2000) 373 [hep-ex/0004005];
L3 collaboration, P. Achard et al., *Measurement of the photon structure function F_2^γ with the L3 detector at LEP*, *Phys. Lett.* **B 622** (2005) 249 [hep-ex/0507042];
OPAL collaboration, G. Abbiendi et al., *Measurement of the hadronic photon structure function F_2^γ at LEP2*, *Phys. Lett.* **B 533** (2002) 207 [hep-ex/0202035];
ALEPH collaboration, A. Heister et al., *Measurement of the hadronic photon structure function $F_2^\gamma(x, Q^2)$ in two-photon collisions at LEP*, *Eur. Phys. J.* **C 30** (2003) 145.

[35] OPAL collaboration, G. Abbiendi et al., *Measurement of the low-x behavior of the photon structure function F_2^γ*, *Eur. Phys. J.* **C 18** (2000) 15 [hep-ex/0007018]; *Inclusive jet production in photon-photon collisions at $\sqrt{s_{ee}}$ from 189 to 2009 GeV*, *Phys. Lett.* **B 658** (2008) 185 [arXiv:0706.3282].

[36] ALEPH, L3 and OPAL collaborations and the LEP Working Group for Two-Photon Physics, *Comparison of deep inelastic electron photon scattering data with the HERWIG and PHOJET Monte Carlo models*, hep-ex/0010041.

[37] A. Denner, S. Dittmaier, M. Roth and L.H. Wieders, *Complete electroweak O(α) corrections to charged-current $e^+e^- \to 4$ fermion processes*, *Phys. Lett.* **B 612** (2005) 223 [hep-ph/0502063].

[38] A. Sommerfeld, *Atombau und Spektrallinien*, vol. 2, Vieweg, Braunschweig Germany (1939);
A.D. Sakharov, *Interaction of an electron and positron in pair production*, *Zh. Eksp. Teor. Fiz.* **18** (1948) 631 [*Sov. Phys. Usp.* **34** (1991) 375].

[39] A.H. Hoang et al., *Top-antitop pair production close to threshold: synopsis of recent NNLO results*, *Eur. Phys. J. direct* **C 2** (2000) 1 [hep-ph/0001286];

JHEP09(2008)076

M. Beneke, A. Signer and V.A. Smirnov, *Top quark production near threshold and the top quark mass*, *Phys. Lett.* **B 454** (1999) 137 [hep-ph/9903260];
A.H. Hoang, A.V. Manohar, I.W. Stewart and T. Teubner, *A renormalization group improved calculation of top quark production near threshold*, *Phys. Rev. Lett.* **86** (2001) 1951 [hep-ph/0011254]; *The threshold $t\bar{t}$ cross section at NNLL order*, *Phys. Rev.* **D 65** (2002) 014014 [hep-ph/0107144];
A.H. Hoang, *Three-loop anomalous dimension of the heavy quark pair production current in non-relativistic QCD*, *Phys. Rev.* **D 69** (2004) 034009 [hep-ph/0307376];
A.A. Penin, A. Pineda, V.A. Smirnov and M. Steinhauser, *Spin dependence of heavy quarkonium production and annihilation rates: complete next-to-next-to-leading logarithmic result*, *Nucl. Phys.* **B 699** (2004) 183 [hep-ph/0406175];
A. Piñeda and A. Signer, *Heavy quark pair production near threshold with potential non-relativistic QCD*, *Nucl. Phys.* **B 762** (2007) 67 [hep-ph/0607239].

[40] Y. Schröder, *The static potential in QCD to two loops*, *Phys. Lett.* **B 447** (1999) 321 [hep-ph/9812205].

[41] A. Billoire, *How heavy must be quarks in order to build coulombic $q\bar{q}$ bound states*, *Phys. Lett.* **B 92** (1980) 343;
Y. Sumino, K. Fujii, K. Hagiwara, H. Murayama and C.K. Ng, *Top quark pair production near threshold*, *Phys. Rev.* **D 47** (1993) 56.

[42] M.E. Luke, A.V. Manohar and I.Z. Rothstein, *Renormalization group scaling in nonrelativistic QCD*, *Phys. Rev.* **D 61** (2000) 074025 [hep-ph/9910209];
A.V. Manohar and I.W. Stewart, *The QCD heavy-quark potential to order v^2: one loop matching conditions*, *Phys. Rev.* **D 62** (2000) 074015 [hep-ph/0003032];
A.H. Hoang and I.W. Stewart, *Ultrasoft renormalization in non-relativistic QCD*, *Phys. Rev.* **D 67** (2003) 114020 [hep-ph/0209340].

[43] A. Piñeda and J. Soto, *Effective field theory for ultrasoft momenta in NRQCD and NRQED*, *Nucl. Phys.* **64** *(Proc. Suppl.)* (1998) 428 [hep-ph/9707481];
A. Piñeda, *Renormalization group improvement of the NRQCD Lagrangian and heavy quarkonium spectrum*, *Phys. Rev.* **D 65** (2002) 074007 [hep-ph/0109117]; *Next-to-leading-log renormalization-group running in heavy-quarkonium creation and annihilation*, *Phys. Rev.* **D 66** (2002) 054022 [hep-ph/0110216].

[44] A.H. Hoang and P. Ruiz-Femenía, *Renormalization group analysis in NRQCD for colored scalars*, *Phys. Rev.* **D 73** (2006) 014015 [hep-ph/0511102].

[45] A. Piñeda and A. Signer, *Renormalization group improved sum rule analysis for the bottom quark mass*, *Phys. Rev.* **D 73** (2006) 111501 [hep-ph/0601185].

[46] A. Arhrib and W. Hollik, *Radiative corrections to scalar-fermion pair production in high energy e^+e^- collisions*, *JHEP* **04** (2004) 073 [hep-ph/0311149];
K. Kovařík, C. Weber, H. Eberl and W. Majerotto, *Full O(α) corrections to $e^+e^- \to \tilde{f}_i\tilde{f}_j$*, *Phys. Rev.* **D 72** (2005) 053010 [hep-ph/0506021].

[47] C. Balázs, M.S. Carena, A. Menon, D.E. Morrissey and C.E.M. Wagner, *The supersymmetric origin of matter*, *Phys. Rev.* **D 71** (2005) 075002 [hep-ph/0412264].

[48] The Planck collaboration, *The science case of Planck* (2005), *ESA-SCI* (2005) 1 available at http://www.rssd.esa.int/index.php?project=Planck;
See also *ESA Science & Technology: Planck homepage*,
http://planck.esa.int/science-e/www/area/index.cfm?fareaid=17.

JHEP09(2008)076